

Optical Characterization and Evaluation of Dye-Nanoparticle Interactions

Annette Casandra Booker

Thesis submitted to the faculty of the Virginia Polytechnic Institute and State University in
partial fulfillment of the requirements for the degree of

Master of Science
In
Electrical and Computer Engineering

Dr. Kathleen Meehan, Chair
Dr. Guo-Quan Lu, Member
Dr. Wayne Scales, Member

May 10, 2006
Blacksburg, Virginia

Keywords: nanoparticle, surface plasmon resonance, resonance energy transfer, Mie theory

Copyright 2006

Optical Characterization and Evaluation of Dye-Nanoparticle Interactions

Annette Casandra Booker

ABSTRACT

Surface plasmon resonance has become a widely investigated phenomenon in the past few years. Initially descriptive of light interactions with metallic films, research has branched out to encompass the nanoparticles as well. Generation of the maximum surface plasmon resonance for nanostructures is based on the resonance condition that the oscillatory behavior of the 'free' electrons on the surface of the particle become equivalent to the frequency of the excitation light; for films this required a specific geometry.

Metallic nanoparticles have also interested researchers because of their unique optical properties. Depending on the metal, observations of quenching as well as fluorescence enhancement have been reported. Based on the phenomenon of surface plasmon resonance as well as the properties of metallic nanoparticles, this research reports the interaction of gold and silver nanoparticles in an aqueous dye solution. Our research is the basis for developing an optical sensor used for water treatment centers as an alarm mechanism. Due to the inefficiency of the fluorophore used in similar optodes, sufficient fluorescence was not obtained. With the addition of the nanoparticles, we hoped to observe the transfer of energy from the nanoparticle to the fluorophore to increase the overall intensity, thereby creating a sufficient signal.

Using the excitation theories discovered by Raman, Mie, and Forster and Dexter as our foundation, we mixed a strongly fluorescent dye with gold nanoparticles and again with silver nanoparticles. After taken measurements via fluorescence spectroscopy, absorption spectroscopy, and photoluminescence excitation, we observed that the silver nanoparticles seemed to enhance the fluorescence of the dye while the gold nanoparticles quenched the fluorescence.

DEDICATION

This thesis is dedicated in memory of my mother, Toleda Annette Booker (June 29, 1946-October 4, 2001). She was more than a mother; she was a very dear friend. I dedicate this to her memory because of her strength, endurance, character, friendliness, and love. She will always be missed. Thank you, Mom, for the sacrifice of love; heaven has definitely acquired another angel.

I also want to dedicate this paper to the numerous people who have helped me reach this pinnacle of my life: my older sister, Burthia to whom words cannot express my love and admiration. You have been not only my sister but my rock and my voice of reason!

To my friends, especially my JAGM girls, thank you for keeping me grounded. To my extended family, especially my godmother Edna Overton and my Uncle Thomas Leigh, thank you for your inspiring words and support. This experience has been a battle but you all have made the victory sweet for me!

To my family at New Life Worship Center in Norfolk, Virginia, thank you for your continuous support through prayer, guidance, friendship, and phone calls. Without you, my walk would have been lonesome. To my undergraduate institution, Norfolk State University, and specifically to the DNIMAS program (Dozoretz National Institute for Minorities in Applied Sciences), thank you for preparing me to accomplish my dreams; the foundation you have set for me has allowed me to exceed my goals.

Above all, I give all honor and glory to God. You, alone, have made this possible. Thank you for your Grace and Mercy and its guidance throughout my studies. You have shown me miracles beyond what I could have ever known and for that I am eternally grateful.

ACKNOWLEDGMENTS

I would like to thank my thesis advisor, Dr. Kathleen Meehan, for her encouragement as well as the challenges she has given me. Without direction, nothing could have been completed. In addition I would like to also thank Dr. Wayne Scales and Mrs. Cynthia Hopkins for their tireless efforts in helping me achieve my goals; thanks you for not giving up on me.

In addition, I would also like to thank the members of my thesis committee: Dr. Kathleen Meehan, my advisor and chair of the committee, Dr. Guo-Quan Lu, and Dr. Wayne Scales, both members of my committee. Thank you for your support.

TABLE OF CONTENTS

DEDICATION	III
ACKNOWLEDGMENTS	IV
TABLE OF FIGURES	VIII
CHAPTER 1. INTRODUCTION	1
1.1 SURFACE PLASMONS AND SURFACE PLASMON RESONANCE	1
1.2 RATIONALE OF THE STUDY	4
CHAPTER 2. BACKGROUND	6
2.1 THEORIES OF PHOTON-PLASMON INTERACTION	6
2.1.1 <i>Exciting Surface Plasmons</i>	6
2.1.2 <i>Rayleigh Scattering</i>	7
2.1.3 <i>Mie Theory</i>	8
2.1.4 <i>Raman Scattering Theory</i>	10
2.1.5 <i>Förster-Dexter Theory of Energy Transfer</i>	13
2.1.6 <i>Fluorescence Resonance Energy Transfer (FRET)</i>	14
2.1.7 <i>Electric Field Interaction</i>	16
2.2 PLASMON-DYE INTERACTIONS	18
2.2.1 <i>Radiative and Non-Radiative Decay Engineering</i>	18
2.2.2 <i>Energy Transfer</i>	19
2.2.3 <i>Modifications by the Electric Field</i>	21
CHAPTER 3. EXPERIMENTAL PROCEDURE AND RESULTS	25
3.1 SAMPLE PREPARATION	25
3.1.1 <i>Nanoparticle Synthesis</i>	25
3.1.2 <i>Dye Solution Synthesis</i>	26
3.2 OPTICAL CHARACTERIZATION TECHNIQUES	26
3.2.1 <i>Photoluminescence Excitation Spectroscopy</i>	27
3.2.2 <i>Fluorescence Spectroscopy</i>	27
3.2.3 <i>Absorption Spectroscopy</i>	28
3.2.4 <i>Transmission Electron Microscopy (TEM)</i>	29
3.3 EXPERIMENTAL RESULTS	29
3.3.1 <i>Sulforhodamine 101 Characterization and Analysis</i>	29
3.3.2 <i>Gold Nanoparticle Characterization and Analysis</i>	32
3.3.3 <i>Gold-S101 Solution Measurements and Characterization</i>	33
3.3.4 <i>Gold-Dye Analysis</i>	35
3.3.5 <i>Silver Nanoparticle Characterization</i>	36
3.3.6 <i>Silver-S101 Measurements and Characterization</i>	37
3.3.7 <i>Silver-Dye Analysis</i>	37
CHAPTER 4. CONCLUSIONS AND FUTURE WORK	41
BIBLIOGRAPHY	43

TABLE OF FIGURES

Figure 1. Standard Kretschmann configuration of attenuated total reflection.	2
Figure 2. Depiction of light scattering. a.) Rayleigh scattering, b.) Raman scattering with Stokes effect, c.) Raman scattering with anti-Stokes effect. In this case, the molecule absorbs the energy with the Stokes effect while it loses energy with the anti-Stokes effect. E_i refers to the incident energy of the photon while E_f refers to the final energy of the photon after interacting with the molecule.	11
Figure 3. Excitation and recombination mechanism inside the band structure of noble metals. E_F is the Fermi energy and k_F is the Fermi momentum. Mooradian determined that emission occurred from direct recombination of conduction band electrons below E_F with holes in the d band that scattered to momentums less than k_F	23
Figure 4. PLE data for 1ml of S101 diluted in 8ml of DI water.....	30
Figure 5. Photoluminescence data for 1ml of S101 diluted in 8ml of DI water excited at 588nm. Significant fluorescence is noted at longer wavelengths than 605nm.	31
Figure 6. PL data collected when exciting the 1ml of S101 diluted in 8ml of DI water at 550nm. Though significant fluorescence is shown at 605nm, the intensity of the fluorescence is not as substantial as the previous data collected at the excitation of 588nm.....	31
Figure 7. Absorption comparison of known-sized gold nanoparticles and the generated sample.	32
Figure 8. Absorption data obtained for diluted S101 sample. Notice the absorption peaks at 550nm and 588nm. This indicates that maximum absorption occurs at these wavelengths. Data coincides with both the PLE and the PL data collected previously.....	33
Figure 9. Absorption data for 1ml S101 solution with varied concentrations of gold nanoparticles. The legend details the concentration of gold nanoparticles (i.e. A1=1ml of solution containing gold nanoparticles. A2 = 2ml of the gold colloid solution, etc.) for a total sample volume of 9ml. Note that the data was normalized.	34
Figure 10. Absorption data of gold/3ml S101 solution. Though there was not a shift in the data, as expected, there is an increase in the absorbance. Note that the total sample solution is 9ml and the legend indicates the amount of nanoparticles present in the solution (i.e. B1= 1ml gold nanoparticles).....	34
Figure 11. PL data for gold-dye system. Note the excitation wavelength is 544nm and that the peak at 609nm decreases with the addition of the gold nanoparticles.	35
Figure 12. Comparison of absorption data for 20nm silver nanoparticles. Note that the in-house nanoparticles had better monodispersion than the commercially available sample. However due to the lack of aqueous stability, we chose to use the commercially available nanoparticles.	36
Figure 13. Absorption data for the 1ml S101-silver nanoparticle system. Note the secondary peak located at 588nm. This peak is similar to the absorption peak for the S101-only solution. The peak for the silver nanoparticles (414nm) seems to increase in absorbance as the concentration of silver increases.	38

Figure 14. PLE data for the dye-silver nanoparticle solution with 1ml of S101 and 2 ml of silver nanoparticles. Notice that the maximum excitation peak is still found at 588nm with a secondary peak at approximately 550nm for fluorescence at 609nm.....	39
Figure 15. PL data for the silver-dye sample. Notice that excitation at 580nm gives significant fluorescence at 609nm. It should be noted that for the excitation wavelengths of 514nm and 544nm (determined from PLE data), the peaks at those wavelengths indicate scattering of the excitation wavelength.....	40

CHAPTER 1. INTRODUCTION

Applications of metallic colloids have become more and more prevalent in the past few decades.^[1-3] Colloids, in general, consist of tens to hundreds of thousands of atoms, having a diameter of tens to hundreds of nanometers while nanoparticles consist of small clusters or large collections of molecules (around the 1nm diameter size). Colloids, unlike nanoparticles, are also usually found in an aqueous medium.^[3] In the past few years, however, the meanings for these two terms, colloids and nanoparticle, have become synonymous because of the similarities in the chemical synthesis of them both; now all particles that fall into the range of 10^{-9} meters are considered “nanoparticles”.^[3]

Nanotechnology is the study of structures on the nanometer size scale, providing an opportunity to synthesize materials with high nonlinearities while tuning the optical properties by varying size and shape.^[1,3,4] these dependencies will be discussed later with the nanoparticle properties. The technology and study of nanoparticle structures has sparked changes in medicine and optics because of their optical and catalytic behavior, setting the foundation of the study of light with nanometer structures (nanophotonics).^[1, 3-6]

Optically, noble metallic nanoparticles, primarily gold and silver nanoparticles, have attracted considerable attention.^[1-3] Nanoparticle and colloidal chemistry have provided a means of characterizing a transitional stage from individual atom chemistry to bulk matter.^[3] A focus on colloidal chemistry and the behavior of these metallic nanoparticles has paved the way to a new field of research: plasmonics.^[4, 7] Plasmonics, in general, is the result of optical excitations of the ‘free’ electrons within the conduction band can causing collective oscillations. This induction of oscillations is termed surface plasmon resonance (SPR).^[4] Using this phenomenon as the foundation of her research, the author will review the properties, mathematics, and applications of surface plasmon resonance and fluorescence detection.

1.1 Surface Plasmons and Surface Plasmon Resonance

Surface plasmons are electromagnetic waves that propagate along a metal-dielectric interface.^[4] A simplified definition of a surface plasmons is the excitation of the surface electrons of a metal by an incident light source. The intensity of the electric field of a surface plasmon decays exponentially as the distance from the metal-dielectric interface increases.^[4,5]

When the incident photon energy is resonant with the oscillation frequency of the “free” electrons on a metallic surface, surface plasmon resonance (SPR) is achieved. The most common means of excitation is achieved through the Kretschmann configuration shown in Figure 1; this configuration depends on attenuated total reflection in order to excite the surface plasmon resonance.^[4] To induce the surface plasmon resonance, a specific incident angle of light with respect to the metal-dielectric interface must be achieved. At this angle (θ_{SP}), the electromagnetic wave interacts with the electrons at the metal-dielectric interface and generates a surface plasmon.^[4] Equation 1 gives the relationship between the angle needed to generate a surface plasmon (θ_{SP}), the wavevector of the surface plasmon (k_{SP}), the wavevector of the bulk electromagnetic wave (k), and the refractive index of the glass prism (n_p). We note that the Kretschmann geometry is only used to excite surface plasmons on planar or flat surfaces along a metal-dielectric interface. In the case of metallic nanoparticles, SPR is achieved differently; since the oscillations are localized, the wavevector k_{SP} is not needed. Consequently, surface plasmons related to metallic nanoparticles are termed localized surface plasmons.

$$k_{SP} = kn_p \sin \theta_{SP} \quad (1)$$

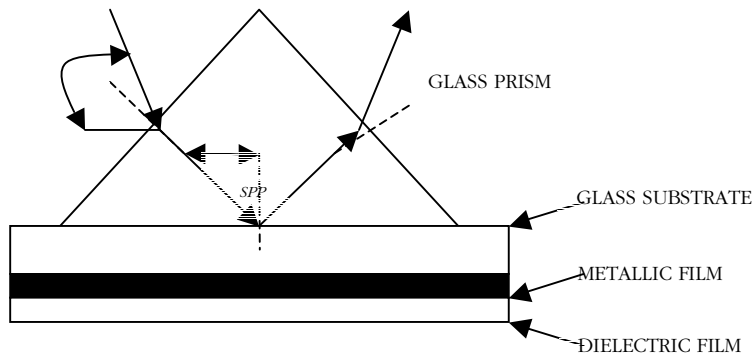


Figure 1. Standard Kretschmann configuration of attenuated total reflection.

To understand the phenomenon of surface plasmon resonance (SPR), consider the propagation constant of the electromagnetic wave in the metal along the metallic surface. For a metallic film, the electromagnetic field is defined by the complex wavevector given by Equation 2. The propagation constant to achieve surface plasmon resonance (k_{SP}) is given by Equation 3.^[8] ϵ_m and ϵ are the dielectric constants of the metal and the evanescent field, respectively. Ω is the angular frequency of the incident light and c is the speed of light.^[3,8] Since the real component of the metallic dielectric constant is substantially larger than the imaginary component, the propagation constant can be estimated by Equation 4.^[8] For nanoparticles, surface plasmon resonance is achieved when k_{SP} is equivalent to the wavevector of the incident light.^[8-10]

$$k_x = k_r + ik_{im} \quad (2)$$

$$k_{SP} = \frac{\omega}{c} \left(\frac{\epsilon_m \epsilon}{\epsilon_m + \epsilon} \right)^{1/2} \quad (3)$$

$$k_{SP} = \frac{\omega}{c} \left(\frac{\epsilon_r \epsilon}{\epsilon_r + \epsilon} \right)^{1/2} \quad (4)$$

Metallic nanoparticles also differ from semiconductor quantum dots in many ways including the means of modifying the optical spectra. While quantum dots require the quantization of electron and hole energy levels via quantum confinement in order to modify the optical spectra, metallic nanoparticles use light absorptive properties and the induction of surface plasmon resonance to modify the optical spectra. The absorption is the resultant of the collective oscillation of electrons induced by the interaction with the localized electromagnetic field; these oscillations produce surface plasmon waves. The specific wavelengths that induce these surface plasmon oscillations are termed plasmon bands.^[3,4,10] In addition, intraband transitions, which allow the promotion of an electron from the conduction band, or a hole from the valence band from one energy level to another, could lead to enhanced fluorescence or absorption, as will be seen later, with gold and silver nanoparticles.^[2, 3, 7, 11, 12] It should also be noted that the generation of localized surface plasmon resonance on metallic nanoparticles require no specific configurations (i.e. Kretschmann geometry used on planar surfaces).^[4]

Surface plasmon resonance can also be used in fluorescence detection. Under certain conditions noted above, the incident light is able to induce surface plasmon resonance and create an electric field. With this in mind, we expect that an excited fluorescent dye molecule could also excite a surface plasmon and create a radiative beam; this phenomenon is termed surface plasmon-coupled emission.^[8] The wavelengths needed to excite the surface plasmons in these coupled systems of fluorophores and metallic nanoparticles are different as well; these differences arise from the addition of the properties of the fluorescent dye. It should be noted that fluorophores emit without recalling the source of its excitation and therefore has no plane of incidence for the plasmon-coupled emission.^[8] This implies that fluorophores can be excited directly or indirectly^[4,8] (i.e. energy transfer, electric field excitation, resonance energy transfer) from a metallic nanoparticle. The mechanisms of all of these methods of excitation are discussed in Chapter 2.

1.2 Rationale of the Study

As mentioned previously, the new field of plasmonics has a variety of optical applications. Biological sensing devices, or simply biosensors, as well as polymer sensors are just a few of the applications that benefit from plasmonics. Previous studies^[3,5, 13-15] have recognized the need for combining biological components such as DNA and proteins with metallic nanoparticles or thin films to achieve enhancement of the device signal.^[5] Metallic nanoparticles present unique opportunity to use exploit the optical and electronic properties that bulk materials do not possess.^[14] We will discuss these properties in Chapter 2 and display their unique properties in the experimental section found in Chapter 3.

Sensing devices for water treatment systems have become quite demanding as well.^[16, 17] Changes to water quality and defects in waste management have proven to be quite hazardous to the environment as well as human health.^[16] Current environmental sensors^[13, 14] utilize a fluorescent dye in a polymer matrix in order to create an optode or optical ion-selective sensor. These sensors are limited by the low sensitivity and weak signal given by the fluorescent dye interaction. Our research proposes to determine the appropriate conditions to optimize the enhancement of the absorption signal in the presence of a dye by utilizing metallic nanoparticle optical properties and the interaction of the metal-dye system.

This investigation was launched after searching for materials with unique properties that are modified when in the presence of specific molecules for a variety of applications, including biosensors and optical sensing devices. We note that our original dye system (chromoionophore I) was replaced with sulforhodamine 101 (S101) due to the lack of the availability of the former dye as well cost. In addition, since the S101 shared many of the properties of the chromoionophore, our research can be correlated and later expanded to incorporate this potassium-sensitive dye. We describe the system in Chapters 3 and 4.

CHAPTER 2. BACKGROUND

2.1 Theories of Photon-Plasmon Interaction

This chapter identifies the theories that describe the behavior of a photon in a system when it encounters a plasmon. Recall that surface plasmons waves, defined as oscillations of free electrons in a film, layer, or aqueous solution, are induced through an interaction between a photon and free electrons in this same layer, film, or solution. The maximum transfer of energy occurs when the surface reflectivity of the metal decreases, an indication of the photon flux to the surface plasmon wave (i.e. the absorption of the incident light at a particular angle of incidence). Note that this condition is fulfilled within a certain range of wavelengths. The outcome of this phenomenon is surface plasmon resonance.

Three methods presented to describe the excitation of the surface plasmon oscillation: The Forster-Dexter theory of energy transfer, the Mie theory, and the Raman scattering theory.

2.1.1 Exciting Surface Plasmons

The basis of this research is to determine the proper parameters to excite surface plasmons in order to characterize its behavior in a dye solution. In Chapter 1, we noted that surface plasmons are charge density waves that propagate along a metallic surface. In order to generate a surface plasmon, an evanescent wave is produced. This wave penetrates the metallic surface and oscillates the electron at the metal-dielectric surface causing surface plasmon resonance (SPR). Mathematically, SPR occurs when the wave vector component of the surface plasmon equals the wave vector of the incident light ^[9]:

$$k_{light} = k_{SP} \quad (1)$$
$$\frac{2\pi}{\lambda} n_p \sin(\theta) \cong \frac{2\pi}{\lambda_p} \sqrt{\frac{\epsilon_{mr} n_s^2}{\epsilon_{mr} + n_s^2}}$$

where k is a wavevector. The second equation explicitly explains the relationship between the components that make up the wavevector: n_p is the refractive index of the prism coupler, ϵ_{mr} is the real portion of the dielectric constant of the metal, λ is the incident wavelength, λ_p is the wavelength of the surface plasmon, and θ is the angle of incidence. The refractive index, dielectric constant, and the wavelength of the surface plasmon are constants, varying according to the type of sample used; the angle and wavelength of incidence are the variable components that alter the

surface plasmon resonance. Since the dielectric constant of a metal is complex, the surface plasmon wave is also complex. In addition, the dielectric function relies heavily on the wavelength of the incident light, influencing the overall surface plasmon resonance. ^[9]

For metallic particles, exciting surface plasmons also depends on the polarizability of that particle. Polarizability, α , is defined as the ability to induce a dipole moment, μ_{in} , using an applied electric field, E . ^[10]

$$\mu_{in} = \alpha E \quad (2)$$

In general, exciting a material system is based on the scattering of light by particles. Scattering, a process that can operate with up to two photons, occurs when incident light is transmitted through a system; a portion of the light leaves the system with unchanged frequency or energy while a smaller portion can be scattered. The intensity and polarization of specific scattered light is dependent on the direction of the observation; recall that scattered radiation can be observed in all directions. These observations will also determine that scattered light has characteristics associated not only with the incident source but also with new combinations of frequencies generated from photon interaction. ^[18]

The Mie, Raman scattering, and Förster-Dexter energy transfer theories detail specific methods of exciting surface plasmons in a system via scattering. Differences between Rayleigh scattering and these theories will also be discussed to set the foundation of the research.

2.1.2 Rayleigh Scattering

Rayleigh scattering theory addresses the scattering of light, or other electromagnetic radiation, by particles less than the wavelength of the incident light source; this theory was first analyzed and developed by Lord Rayleigh who wanted to investigate the reason for the sky's blue color. From this initial curiosity, Rayleigh studied transparent solids and liquids and how light interacted with these mediums. He observed that incident light could scatter in the medium and exit without changing frequencies. He also determined that the intensity of the scattered light is the inverse fourth power of the wavelength; this later became the Rayleigh law. Even with his success, Rayleigh's discovery and theory was still limited: particles larger than approximately one-tenth of the wavelength of light could not be characterized by his theory. Instead, many years later, Gustav Mie developed the Mie theory which offered a means of characterizing nanoparticle-light

interactions by observing criteria such as shape and the surrounding medium, and the effects of these parameters on the scattering of light. ^[18, 19]

2.1.3 Mie Theory

Energy transfer describes the method by which a molecule can exchange or transfer its energy to another molecule. In the early 20th century, researcher Gustav Mie began to investigate the behavior of colloidal particles in an aqueous solution in order to characterize these particles by their electrical and optical properties. During this time, Mie developed a theory that mathematically describes the scattering of incident light by spherical particles. Mie's theory, unlike that of his predecessor, Lord Rayleigh, considered the effect of radiation on spheres in general, regardless of the size of the sphere's radius. ^[20]

Mie began his mathematical description by applying spherical coordinates to Maxwell's equations with suitable boundary conditions and parameters such as the particle size, optical characteristics of the particle material, and the optical characteristics of the surrounding medium. With these parameters in place, the solution was found to describe the multipole oscillations for the extinction cross-section of nanoparticles. ^[3, 10] Using series expansion of the electric and magnetic fields, one determines that the extinction coefficient, σ_{ext} , and the scattering coefficient, σ_{scat} , can be defined by the following equations:

$$\begin{aligned}
 \sigma_{ext} &= \frac{2\pi}{|k|^2} \sum_{L=1}^{\infty} (2L+1) \text{Re}(a_L + b_L) \\
 \sigma_{scat} &= \frac{2\pi}{|k|^2} \sum_{L=1}^{\infty} (2L+1) \text{Re}(|a_L|^2 + |b_L|^2) \\
 \sigma_{abs} &= \sigma_{ext} - \sigma_{scat} \\
 a_L &= \frac{m \psi_L(mx) \psi_L'(x) - \psi_L'(mx) \psi_L(x)}{m \psi_L(mx) \eta_L'(x) - \psi_L'(mx) \eta_L(x)} \\
 b_L &= \frac{\psi_L(mx) \psi_L'(x) - m \psi_L'(mx) \psi_L(x)}{\psi_L(mx) \eta_L'(x) - m \psi_L'(mx) \eta_L(x)}
 \end{aligned} \tag{3}$$

where $m=n/n_m$, where n is the complex refractive index of the particle and n_m is the real component of the refractive index of the surrounding medium. k is the wavevector, as stated before, and $x=|k|r$ where r is the radius of the nanoparticle. ψ_L and η_L are the Ricatti-Bessel cylindrical functions (the prime indicates the differentiation with respect to the quantity inside of the parentheses), and the L is the summation of the order of partial waves (i.e. $L=1$ is the dipole field or oscillation, $L=2$

corresponds to the quadropole, etc.) The farther away from a cluster of nanoparticles, the partial waves approach equality with the waves coming from equivalent point multipoles.^[3, 10] Mie also determined that the scalar electromagnetic potentials associated with the particles could be derived from their electric and magnetic fields.^[10] Furthermore, his solution related the interaction of electromagnetic incident light and small spheres with the optical properties of bulk material, specifically the frequency-dependent material dielectric constant.^[3]

Consider nanoparticles that are much smaller than the wavelength of the incident light (i.e. $2r < \lambda_{max}/10$). In this case, according to the calculations from Mie, only the dipole oscillations are characterized and considered significant to the extinction cross-section. The calculation then becomes

$$\sigma_{ext}(\omega) = 9 \frac{\omega}{c} \epsilon_m^{3/2} V \frac{\epsilon_2(\omega)}{[\epsilon_1(\omega) + 2\epsilon_m]^2 + \epsilon_2(\omega)^2} \quad (4)$$

where V is the spherical volume $(4\pi/3)r^3$, ω is the angular frequency of the incident light, c is the speed of light, and ϵ_m and $\epsilon(\omega) = \epsilon_1(\omega) + i\epsilon_2(\omega)$ are the dielectric constants of the surrounding medium and the material, respectively. Note that achieving resonance is dependent upon fulfilling the condition where $\epsilon_1(\omega) = -2\epsilon_m$ but only if $\epsilon_2(\omega)$ is relatively small or weakly dependent on the angular frequency.^[3,10]

Equation 4 has been used to determine the absorption spectra of small metallic nanoparticles (gold nanoparticles with radii of 20nm or less). However, if the nanoparticles' radii are larger than this value, or rather exceed the condition of being less than the wavelength, then the above equation is void and the original equations (Equation 3) apply. Consequently, the resonance becomes dependent on the particle size since x is a function of the radius of the particle r .^[3] Once the particle size exceeds the size of the wavelength, higher order modes of L are needed to define the system; this is because at large sizes the incident light can no longer polarize the light uniformly. These higher modes reach a maximum at lower energies and therefore cause a red shift in the plasmon band (a Stokes shift described later) as the radii increases in size. These observations follow Mie's theory on scattering and explained the determination of the red coloring associated with nanoparticles in aqueous solution.^[3,10,20]

Note that Mie's theory is limited to systems that, generally, have low concentrations of nanoparticles and assumes that these particles are non-interacting and separated, one from another. This assumption further assumes that the electric field generated by exciting a surface plasmon

resonance associated with a single nanoparticle does not interact with its surrounding counterparts. Should the particles become close in proximity to one another, a red shift occurs in the plasmon resonance and a secondary absorption peak, at longer wavelengths, is observed.

2.1.4 Raman Scattering Theory

The Raman scattering theory was discovered by C.V. Raman and his student K.S. Krishnan. The theory, based on both Rayleigh scattering and the Compton effect, is defined as the inelastic scattering of photons which can generate or destroy an optical phonon. In the case of surface plasmon resonance, the Raman scattering theory, a two photon process, states that a photon is absorbed from the incident source and reemitted at an intermediate electron energy level. The additional energy is then transferred to the molecule. This secondary photon, which has lower energy than the primary photon, generates a Stokes line on the red side of the incident spectrum. The frequency of the scattered light is dependent upon the characteristics of the system (i.e. nanoparticle or dye molecule). [2,4,9]

Generally, if the scattered light has unchanged frequency, it is considered to be Rayleigh scattering; however, if there is a change in frequency, as stated before, it is considered Raman scattering. The observation of these newly generated frequencies within a spectrum are collectively called the Raman spectrum; individually, these frequencies are termed Raman lines or bands. Further analysis determines that Raman bands at frequencies less than the incident frequency are considered to be Stokes bands or lines; consequently, frequencies greater than the incident frequency are deemed anti-Stokes lines. (Recall that Stokes law states that the frequency of fluorescent light is always less than or equal to the source frequency. Therefore, Stokes lines correspond to attributes associated with Stokes' law while anti-Stokes lines dispute Stokes's law.) [18] The nomenclature is maintained though Raman scattering is different from fluorescent properties (Figure 2).

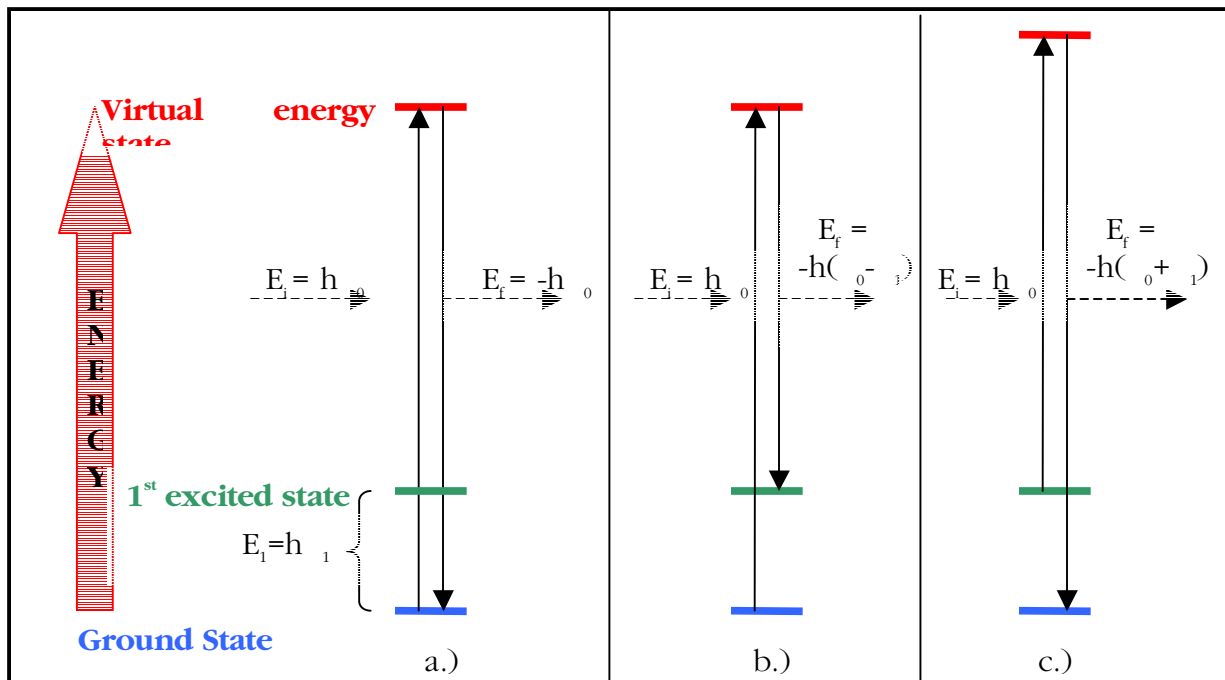


Figure 2. Depiction of light scattering. a.) Rayleigh scattering, b.) Raman scattering with Stokes effect, c.) Raman scattering with anti-Stokes effect. In this case, the molecule absorbs the energy with the Stokes effect while it loses energy with the anti-Stokes effect. E_i refers to the incident energy of the photon while E_f refers to the final energy of the photon after interacting with the molecule. ^[19]

As mentioned previously, Raman scattering is based on a transfer of excess energy from a photon to a molecule. Consider a model that demonstrates electromagnetic radiation. Prior to excitation there are n_i photons with individual energies of $\hbar\omega_i$, where ω_i is the frequency of the incident light, and the molecule has an initial energy, E_i . Upon interaction between the photon and the molecule, a single photon is destroyed while another photon with energy $\hbar\omega_s$ is generated; the molecule now has a final energy, E_f . The incident source now contains one less photon ($n_i - 1$) with energy $\hbar\omega_i$ and one photon with transition energy of $\hbar\omega_s$. Note that because the energy $\hbar\omega_i$ is not associated with any type of electronic transition energy nor is the photon with this energy absorbed, the conservation of energy in this phase does not apply. Instead, the incident light is used to perturb the molecule in order to present an opportunity for alternative interactions other than direct absorption. ^[18] Note, however, that if $\hbar\omega_i$ begins to approach a electronic transition energy, the intensity of the scattering is enhanced.

Surface enhanced Raman scattering (SERS) was first discovered in the early 1970s. The foundation of SERS relied on two types of interactions between a metallic particle and a molecule: (1) electromagnetic interaction or (2) chemical interaction. Chemical interaction is described as

the combination of molecular and metallic states while the electromagnetic interaction used the electric field from a surface plasmon with the transition moment of an adsorbed molecule; the latter interaction has a larger probability of occurring, especially when used to describe systems that contained metallic island films, encapsulated particles, and aggregated colloids. ^[2]

The electromagnetic approach is derived from the superposition of the incident and scattered electromagnetic fields when these fields interact with the transition moment of a molecule near the surface of a metallic particle. Localized field effects from the metallic particle strengthen the electromagnetic fields near the surface. Recall that the cross section of Raman scattering requires that the transition moment be raised to the fourth power and that the magnification of the electromagnetic field can increase the scattering substantially. Using this information, Franzen^[2] derives an equation for the Raman scattering cross section:

$$\sigma_R = \frac{8\pi\omega_s^3\omega_0M_{if}^4}{9\hbar^2c^4} \left(\int_0^\infty \langle f | i(t) \rangle \exp\{i(\omega_i + \omega_0)t - \Gamma t\} dt \right)^2 \quad (5)$$

σ_R is the Raman scattering cross section, M_{if} is the transition moment of the molecule, ω_0 is the incident light frequency, ω_s is the frequency of the scattered light, ω_i is the ground state vibrational frequency, and Γ is the damping constant. A similar equation can be derived to define the absorption cross section.

$$\sigma_A = \frac{2\pi\omega_0M_{if}^2}{3\hbar c} \int_{-\infty}^\infty \langle i | i(t) \rangle \exp\{i(\omega_i + \omega_0)t - \Gamma t\} dt \quad (6)$$

Note that though the transition moment in this equation has decreased by a factor of two, the probability of either occurrence of absorption or resonant Raman scattering depends on the intensity of the incident light and the square of the incident radiation field, where the intensity, I , is defined as

$$I = \frac{1}{2\epsilon_0 c E_0^2} \quad (7)$$

and E_0 is the amplitude of the incident radiation electric field. ^[2] Enhancing this electric field can lead to an increase in the transition probability (i.e. the elevation of an electron from ground state to a higher energy state occurs quicker). For spherical metallic (i.e. gold or silver) nanoparticles, the radial and tangential electromagnetic fields can be described mathematically as

$$\begin{aligned}
E_t^2 &\propto 2E_0^2[1-g]^2 \\
E_r^2 &\propto 2E_0^2[1+g]^2 \\
g &= \frac{(\varepsilon - \varepsilon_0)}{(\varepsilon + 2\varepsilon_0)}
\end{aligned}
\tag{8}$$

where g is a factor that corresponds to the polarizability of a metal sphere with dielectric constant ε , in a medium with a dielectric constant of ε_0 . Recall that scattering of incident light is related to the polarizability of a metallic particle. As surface plasmon resonance is approached, the dielectric constant approaches a $-2\varepsilon_0$ and g is magnified in order to reach resonance criteria.

2.1.5 Förster-Dexter Theory of Energy Transfer

Over 50 years ago, Förster and Dexter's theory became the foundation of understanding the behavior of resonant energy transfer in solids: luminescence, quenching, and fluorescence depolarization.^[21] The theory was first derived by Förster who wanted to understand the excitation relationship between two organic molecules with large dipole transition moments.^[22] Later, Dexter used Förster's theory as the foundation to describe the effects and behaviors of multi-pole energy transitions (i.e. quadrupole-dipole, dipole-quadrupole, and quadrupole-quadrupole) in inorganic species.^[21-23]

The Förster-Dexter model consists of a single donor and a single acceptor imbedded in a non-conductive matrix. The theory assumes that the excited donor only has two modes of energy decay, radiationless emission or resonance energy transfer to the acceptor, with a higher probability of the latter occurring more frequently than the former; this assumption agrees with the dipole relaxations that occur in the initial state of the donor and the final state of the acceptor, localizing the excitation.^[21,23] The theory can be further described using Fermi's Golden Rule, assuming the following criteria are applicable: (1) the time taken to transfer energy is longer than the documented phonon relaxation times; (2) the Stokes' shifts of both the acceptor and the donor are large enough to prevent back transfer from the donor emission; and (3) donor and acceptor concentrations are small enough that donor-donor and acceptor-acceptor interactions are negligible, only allowing the interaction between a donor and its nearest-neighbor acceptor. Though the latter criterion is rarely met, the Golden Rule is still applicable.^[21]

Assuming that a single excited donor only operates in the energy emission mode mentioned previously, it can be assumed that the donor and acceptor have some relation to

emission and absorption data. Furthermore, using these assumptions, Förster and Dexter theorized that a critical transfer distance separation can be determined mathematically. This distance describes the length in which a single donor can be separated and undergo both radiationless emission as well as resonant energy transfer to its nearest-neighbor acceptor ^[22]:

$$\bar{P}_{DA} = \left(\frac{1}{\tau_D} \right) \left(\frac{R_{dipole-dipole}^6}{R^6} \right) \quad (9)$$

where τ_d is the donor emission lifetime and R is the separation distance between donor and acceptor. $R_{dipole-dipole}$ is further expanded in a differential equation that accounts for the area under the acceptor absorption band in terms of its cross section (Q_a^0), the acceptor absorption normalized to unity ($F_a(E)$), the normalized donor emission ($f_d(E)$), and the speed of light in vacuum (c), which verifies and relates the separation distance to the absorption and emission data. It should be noted that the following equation is only applicable if the separation distance, R , is large enough to discount the wavefunctions of other associated impurities (dipoles) which corresponds to the first condition for using the Fermi Golden Rule. ^[21,22]

$$R_{dipole-dipole}^6 = \int \frac{9\hbar^4 c^4}{8\pi} \frac{\Phi_{dipole-dipole}^2}{\epsilon^2} Q_a^0 \frac{f_d(E)F_a(E)}{E^4} dE \quad (10)$$

The Förster-Dexter theory is not without its limitations however. Because of its dependence on donor-acceptor separation distances and the criteria behind Fermi's Golden Rule, the Förster-Dexter theory is limited to systems where there are large distances between the donor and acceptor, implying an extremely weak coupling of the two impurities. ^[21, 23] In order to maintain the theory, however, Dow states that the intervening impurities (non-targeted donors and acceptors) must be medium-like, especially in the case of multi-dipole interactions. Dow, with the assistance of Kohn *et al.*, further theorizes that though the large separation of donors and acceptors allows the intervening impurities to interfere with the energy transfer of a targeted donor to a targeted acceptor, if the impurities are similar to the surrounding media, their effects can be substituted by the donor or acceptor induced electromagnetic field characterized by a wave-number- and frequency-dependent dielectric function. ^[21]

2.1.6 Fluorescence Resonance Energy Transfer (FRET)

Fluorescent resonance energy transfer, also termed single-paired Förster resonance energy transfer, describes the behavior described previously: the interaction of an acceptor molecule with

a donor molecule; the original experiments dealt with two fluorophores. In order to have an efficient process, three considerations are given: 1.) the distance between the donor and the acceptor, 2.) the spectral overlap of the donor emission spectrum and the acceptor absorption spectra, and 3.) the relative orientation or alignment of the excited donor dipole moment and the ground state acceptor dipole moment. ^[24] Again, as mentioned previously, the energy transfer occurs after the induction of a dipole moment in both the acceptor and the donor.

Upon excitation from an incident light source, the acceptor molecule becomes excited, and if the donor molecule is nearby, the energized acceptor molecule is able to transfer its energy to the donor. During the transfer of energy, the donor experiences a decrease in its fluorescent intensity while its excitation lifetime increases; simultaneously, the donor's emission intensity is increased. Förster describes this efficiency mathematically using the following equation.

$$E = \frac{1}{(1 + [R/R_0]^6)} \quad (11)$$

R is the separation distance between the acceptor and donor while R_0 is the distance at which approximately 50% of the energy is transferred and is a function of the properties of dyes and the orientation of their individual dipole moments; R_0 is measured in angstroms with typical values of 10-80 Å. ^[22, 24, 25]

$$R_0 = [8.79 \times 10^{-5} J(\lambda) \phi_D n^{-4} \kappa^2]^{1/6} \quad [\text{Å}] \quad (12)$$

$J(\lambda)$ is the spectral overlap of the emission and absorption spectra [$\text{nm}^4 / (\text{M cm})$], ϕ the donor quantum yield, n is the refractive index of the medium, and κ^2 is a geometrical factor describing the orientation of the dipoles. ^[25] By definition, the transfer efficiency is the ratio of the transfer rate to the sum total of the rates of all deexcitation processes (i.e. fluorescence, phosphorescence, vibrational relaxation, etc.). ^[26]

$$\text{efficiency} = E = \frac{k_T}{k_T + k_f + k'} \quad (13)$$

k_T is the transfer rate between the ground state donor and the excited acceptor, k_f accounts for the deexcitation due to fluorescent emission, and k' represents the summation of all other types of deexcitation methods.

The conventional method of measuring FRET compares the donor sample intensity of the donor only system to the intensity of the donor-acceptor system. In addition, measurements are taken of the acceptor only system and compared to the donor-acceptor system. Theoretically, this

method is possible but experimentally issues with matching concentrations occur; alternatively, measurements of excitation lifetimes are taken. Therefore, FRET efficiency are now determined experimentally from the relative quantum yields, fluorescence intensities, or determining the lifetime of the donor in the donor system only versus the donor-acceptor system.

$$E = 1 - \frac{F_{da}}{F_d} \quad (14)$$

$$E = 1 - \frac{\tau_{da}}{\tau_d}$$

F_{da} in equation 14 represents the donor fluorescence intensity in the presence of the acceptor, F_d represents the donor fluorescence intensity at a given wavelength in the absence of the acceptor, τ_d and τ_{da} represent the donor lifetimes in with and without the presence of the acceptor, respectively. If the acceptor is also fluorescent, its contributions are applied to the above equations. The acceptor's fluorescence, however, is not required to achieve energy transfer, and is therefore, not described. [22]

Though many calculations are given to substantiate the appropriate distances to achieve FRET as well as a solution to determining the efficiency experimentally, values for the geometric orientation are more difficult to quantify and verify. The uncertainty of this factor has been vastly minimized with the onset of new technological approaches and estimations including 1.) using polarized emission data to define the mobility of the donor and the acceptor bound to a substrate while estimating the orientation factor, 2.) selecting donor and acceptor molecules with minimally limited polarization properties, and 3.) using statistical analysis of the energy transfer data to determine the limits of the donor-acceptor distance. Another method used describes the orientation factor by incorporating the angle between the emission dipole of the donor and the absorption dipole of the acceptor, θ_T .

$$\kappa^2 = (\cos \theta_T - 3 \cos \theta_d \cos \theta_a)^2 \quad (15)$$

θ_d and θ_a represent the angles between the vector joining the donor and acceptor and the emission and absorption, respectively. [22]

2.1.7 Electric Field Interaction

Although surface plasmon resonance can be achieved via energy transfer, as has been extensively described above, it is also described by an electric field interaction. Recall that if an

electric field is incident on a dielectric surface (E_0), the field within the material (E) is equivalent to the product of the dielectric constant (ϵ) of the material and the incident electric field. Note that the dielectric constant of a nonabsorbing material and its corresponding refractive index, n , are related: $n = \sqrt{\epsilon}$. However, the dielectric constants of metallic materials are complex numbers. [8] This difference of optical constants occurs because electrons in dielectric materials are bound to the nuclei or shared in covalent bonds between atoms while metallic materials have free or unbound electrons that can react to incident fields. The free electrons of the metal can readily absorb a broad range of energy. At high frequencies, the incident field creates an oscillation amongst the free electrons in response to the oscillating field. Note that the dielectric constant and refractive index of metallic materials rely on the interaction of the incident frequency (wavelength) and electron mobility. [8]

The imaginary component of the metal's dielectric constant is relatively small and positive and is related to the magnitude of the optical absorption while the real component becomes progressively negative as the wavelength increases. These theoretical interpretations are used to experimentally describe the electron oscillations with the charge opposite of the incident electric field. Subsequently, as the wavelength decreases, the real component of the refractive index, theoretically should become negative, indicating the response of the electrons to much lower frequencies. However, since there are no true negative index materials, we submit that the real component remains positive for metals as well. Perfect conduction, however, is related to the refractive index approaching negative infinity. [8]

To better understand the influence of the electric field on plasmon oscillations, consider an electromagnetic wave propagating along the horizontal axis of a metallic material. Using the definition of the internal electric field given previously in equation 8, $k_x = k_r + ik_{imag}$, where k is the wavevector along the horizontal axis, x . In Chapter 1 we noted that the propagation constant for a surface plasmon is

$$k_{SP} = \frac{\omega}{c} \left(\frac{\epsilon_m \epsilon}{\epsilon_m + \epsilon} \right)^{1/2} = k_0 \left(\frac{\epsilon_m \epsilon}{\epsilon_m + \epsilon} \right)^{1/2} \quad (16)$$

ω is the angular frequency of the incident light, c is the speed of light, ϵ_m and ϵ are the dielectric constants of the metal and the surrounding medium, respectively; ϵ is within the evanescent field. According the previous definitions, we know that the imaginary component of the dielectric

constant is relatively small. Therefore, the propagation constant can be adequately approximated by using only the real component of the dielectric constant, ϵ_r .

$$k_{SP} = k_0 \left(\frac{\epsilon_r \epsilon}{\epsilon_r + \epsilon} \right)^{1/2} \quad (17)$$

Subsequently, when the horizontal (x axis) component of the incident light becomes equivalent to the propagation constant of the surface plasmon, the incident light can excite a surface plasmon. However, to obtain resonance conditions, the magnitude of the horizontal component of the incident light must be equal to or exceed the propagation constant of the surface plasmon. [8]

2.2 Plasmon-Dye Interactions

This section describes the interaction of surface plasmons with a fluorescent dye. The previous section described the interaction of the incident light, the induction of an electric field, and the resulting resonance condition. This section will apply these concepts and theories to the nanoparticle-dye solution, which is the basis of the research. In addition, modifications of the optical properties of dyes, nanoparticles, and dye-nanoparticle systems will be discussed.

2.2.1 Radiative and Non-Radiative Decay Engineering

Fluorescence is a spontaneous emission process, which begins when a molecule at an excited state decays to a lower energy level with the transfer of the difference in the energy between the excited state and lower energy levels to a photon or waveguide mode. The probability of this emission process can be described with Fermi's Golden Rule.

$$\Gamma_{ij} \propto |M_{ij}|^2 \rho(\nu_{ij}) \quad (18)$$

Γ_{ij} is the transition rate between the excited state, i , and the lower-energy state, j , M_{ij} is a matrix element connecting the two levels determined by the wavefunctions associated with the levels, $\rho(\nu_{ij})$ is the density of the optical field at the transition frequency, henceforth termed photonic mode density (PMD). [27]

Significant research has defined key parameters that affect fluorescence including quenching, environmental effects, resonance energy transfer, and rotational motion; these factors were used to describe the structure and motion of molecules interacting with other molecules. [21, 22, 27] In addition, it was determined that the spectral properties of fluorophores could be altered

and/or controlled by rate processes that change the nonradiative decay rates of the excited molecule. ^[28,29] Nonradiative decay is provided through either quenching (described later in this section) or energy transfer (RET). Radiative decay, the spontaneous rate of emitting photons, is not affected by either quenching or RET, however. Emission in free space (i.e. a uniform, non-conductive medium) is determined by the excitation coefficient and the absorption spectrum. In order to alter the radiative rate, and therefore influence the properties of the emission spectrum, metallic particles must be introduced into the medium. Control of the rates of radiative decay is henceforth used to define radiative decay engineering (RDE). ^[28]

As stated before, the ability to modify and control the radiative decay rate has implications for the spectral properties of a fluorophore-metal system. However, before describing this complex interaction, consider a simplified system with fluorophores only. Assuming a homogeneous solution is present, the spectral properties of fluorophores emitting into free space can be described using Maxwell's equations for an oscillating dipole radiating into free space; local field effects are negligible and disregarded because of the comparable size of the fluorophore as opposed to the size of the sample container. ^[28] Upon introducing metallic particles into such a system, Maxwell's equations are no longer valid and must be modified to complete the non-free space solution.

Metallic particles in the vicinity of oscillating fluorophores respond to the motion of the dipole to alter the rate of emission and decreases the distance between the oscillating fluorophores; the latter effect interrupts the amount of radiative energy transferred between particles by absorbing the energy of the light. In addition, the interaction of the light with the metallic surface causes an interaction of the oscillating-dipole fluorophore with the metal. Fluorophores are also affected by the properties of the metal. When the incident light interacts with a metallic surface, it affects the electric field associated with the fluorophore because the induced electric field is caused by the generation of surface plasmons. This effect has the ability to increase or decrease the electric field incident on the fluorophore. ^[28]

2.2.2 Energy Transfer

As mentioned before, energy transfer from a molecule to a fluorophore that enables the molecule to decay via a nonradiative path is termed nonradiative decay. The Förster-Dexter theory and the FRET both describe energy transfer in the previous section. Recall, however, that both theories involved non-conducting molecules and coordinating the dipole moments of an acceptor

and a donor. In the presence of metallic particles or surfaces, fluorophores present one of three reactions: 1.) energy transfer that results in quenching to the metal with a distance dependence of d^3 , which will be discussed later; 2.) amplification of the incident electric field by the metal, thereby causing an increase in the intensity of the emission; or 3.) an increase in the intrinsic radiative decay rate of the fluorophore. ^[28]

Fluorophore lifetime (τ_0) and quantum yield (Q_0) are ascertained using the radiative decay rate (Γ) and the rate of nonradiative decay rate to the ground state energy level (k_{nr}), where the quantum yield is defined by the following equation ^[28, 30]:

$$Q_0 = \frac{\Gamma}{(\Gamma + k_{nr})} \quad (19)$$

and the lifetime, disregarding other quenching effects, is given by ^[28, 30]:

$$\tau_0 = \frac{1}{(\Gamma + k_{nr})} \quad (20)$$

If $k_{nr}=0$ or the quantum yield is unity, the natural lifetime of the fluorophore is the inverse of the radiative decay rate. ^[LA3] Both the natural lifetime and the extinction coefficient are dependent upon the oscillation strength of the energy transitions and the PMD. ^[27, 30] Note that the observed lifetime is altered by the influence of a changing k_{nr} . In the presence of a metal, however, equations 19 and 20 become more complex. The quantum yield (Q_m) and lifetime (τ_m) are now given by the following equation where Γ_m is the radiative rate increase when a metal is nearby ^[30]:

$$Q_m = \frac{\Gamma + \Gamma_m}{\Gamma + \Gamma_m + k_{nr}}$$

$$\tau_m = \frac{1}{\Gamma + \Gamma_m + k_{nr}} \quad (21)$$

As presented in the section on FRET, resonance energy transfer cannot occur in fluorophores unless the spectral properties fall within the Förster distance R . Recall that these distances range from 10-80 Å. ^[22, 24, 25, 27] Previous studies have hypothesized that, within a certain proximity, metallic particles near donor and acceptor molecules can produce an increase in the energy transfer rate by a factor of 100-fold or larger with distances extending to 700Å. ^[30] Unfortunately, there is no documentation to support hypotheses with these parameters. However, Lakowicz ^[30] studied

fluorophores in the presence of silver islands and recorded significant increases in energy transfer between silver islands and a specific dye associated with a decrease in decay rates.

2.2.3 Modifications by the Electric Field

As explained, the properties of metallic nanoparticles can be exploited to manipulate the behavior of fluorophores in their vicinity. Based on their electrical interactions, metals affect the induced quenching and photoluminescence of fluorophores. The electromagnetic process that is responsible for the enhanced fluorescence or absorption as well as additional modifications occurs because the particle has the ability to concentrate electric field lines as well as maintain electromagnetic energy if it is resonantly excited. This section details the distribution of these properties to alter the properties of nearby fluorophores.

2.2.3.1 Quenching

Quenching, by definition, is the decrease in fluorescence intensity. Collisional quenching^[28] and energy transfer^[12, 24, 28] are two processes that result in quenching. Collisional quenching is used to characterize biomolecules and fluorophores. The process of collisional quenching begins with a collision between a quencher molecule and a fluorophore. Upon contact, the quantum yield and lifetimes decrease due to the presence of an additional rate process associated with the depopulation of the excited state, $k_q[\text{Qu}]$, where Qu is the quencher concentration and k_q is the bimolecular rate constant.^[28] However, since there has been no documentation on the effect of metallic nanoparticles on collisional quenching, this process is assumed to have no affect at all on the nanoparticle-dye system research discussed.

Quenching caused by energy transfer has been well documented.^[8,11,28,31] Studies on dye-only systems showed a significant deficiency in their quenching efficiency and photostability, limiting the detection of suitable fluorescence signals. Remember the basis of FRET: an excited donor molecule transfers its energy to an acceptor molecule. Replacing the acceptor molecule with a metallic nanoparticle results in a similar phenomenon; resonant energy transfer takes place and the radiative lifetime of the donor molecule changes. However, note that proper alignment and separation (Förster radii equal to approximately 6-8nm leads to quenching) are necessary to achieve FRET as well.^[24,32] Furthermore, FRET only works if the nonradiative time constant of the surface plasmon is longer than that of the time constant associated with the transfer of energy

and subsequent radiative behavior of in the fluorophore; for most instances the time constant of the SP is shorter allowing for quenching of the fluorescence instead of enhancement.

Dulkeith *et al.* also determined a size dependence for the nanoparticle associated with the energy transfer (energy transfer decreases with increasing nanoparticle size) as well as a significant decrease in the dye's radiative rate.^[31] Dulkeith noted that both effects contribute to the overall quenching that was predicted by Gerstein and Nitzan.^[33] Han *et al.* tested 2 nm, 10 nm, and 20 nm gold nanoparticles in a dye solution. Upon investigating the hypothesis that both energy transfer and electron transfer occurs, as noted in FRET excitation of SPR, Han reports that particles with greater than a 2nm diameter have higher probability and incidence of RET quenching. Resonance energy transfer is also dependent on spectral overlap. Since the absorption spectra from the larger particles overlapped significantly with the emission spectra of the fluorophore, resonance energy transfer dominates the observed quenching. In contrast, nanoparticles with smaller dimensions (<2nm) displayed insufficient overlap and therefore had no significant quenching due to energy transfer.^[32]

2.2.3.2 Photoluminescence

Photoluminescence in noble metals was first observed by Mooradian in 1969.^[3, 34, 35] His study investigated the electrical and optical reactions of bulk copper and gold to both argon and mercury excitation. In both types of excitation, it was determined that the emission peak of these bulk metals was centered near the interband absorption edge and, since there was no observed shift of emission to lower energies, the emission was attributed to direct recombination conduction band electron below the Fermi energy level with the holes in the *d* band (Figure 3).^[34] Recall that Mooradian's research related the radiative recombination of the electron-hole pair to photoluminescence. The incident photons are absorbed into the *d*-band, causing interband transitions, before these same photons release their energy and excite electrons from the completely occupied *d*-band to electronic states above the Fermi energy (Figure 3). As the electrons and holes relax into lower energy states, phonon scattering processes begin while recombination of the electrons and holes creates the observed luminescence.

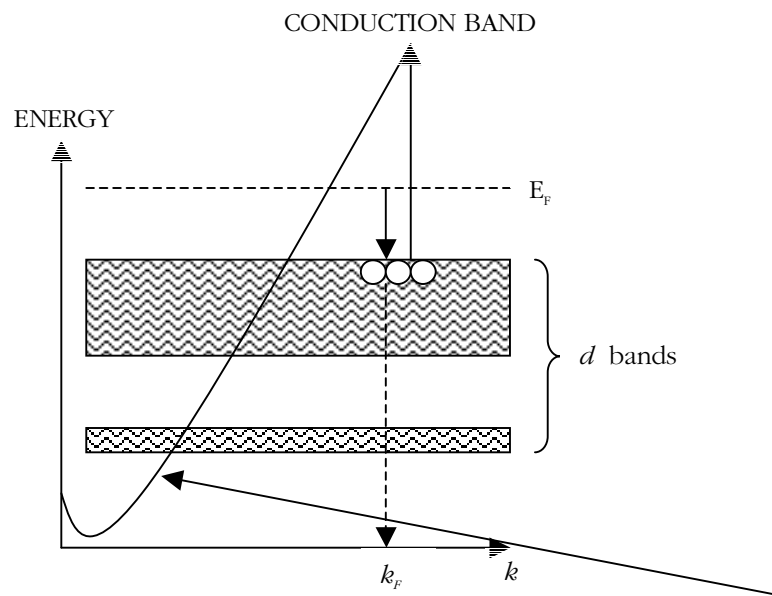


Figure 3. Excitation and recombination mechanism inside the band structure of noble metals. E_F is the Fermi energy and k_F is the Fermi momentum. Mooradian determined that emission occurred from direct recombination of conduction band electrons below E_F with holes in the d band that scattered to momentums less than k_F .^[34]

Mooradian also discovered that the quantum efficiency of the photoluminescence from noble metals was extremely low (usually on the order of 10^{-10}). A later theoretical model developed by Apell and Monreal determined that the overlap of the conduction band and the d band caused a Stokes shift in the luminescence band, thereby affecting the quantum efficiency.^[3, 36]

Expanding Mooradian's research, Boyd *et al.* studied the effects of surface roughness on the photoluminescence properties of noble metals; his study also included the effects on silver.^[3, BOY] Boyd observed the "lightning rod effect", where the luminescence was enhanced greatly and a surface plasmon resonance was induced. The latter observation resulted in an enhanced electric field by the local field induced on the rough surface. Similar effects are found in surface-enhanced Raman scattering (SERS).^[2-3] SERS involves a nanoparticle with absorbed molecules on its surface. Due to the proximity of the molecule and the enhancement of the electromagnetic fields close to a metallic nanoparticle's surface, the nanoparticle is deemed a "nanoamplifier", which increases the Raman signal.^[3]

In the presence of nanoparticles, however, the process of luminescence is modified substantially. It has been established earlier in this chapter that nanoparticles have an induced local

field caused by the surface plasmon resonance.^[3] Link and Boyd theoretically calculated the effect of this photoinduced luminescence on the rough surfaces of noble metal nanorods and nanoparticles. Both hypothesized that the enhancement of the luminescence was due to the combination of local plasmon resonances.^[3,37] Link determined that the photoluminescence increases linearly with increasing square of the length for nanorods of constant width and that there is a linear dependence on the dimensions of the nanorods (both length and width) for the wavelength of the peak emission. Link concluded that the amplified enhancement of the photoluminescence efficiency is a direct result of the enhancement of the field of the incident light and the outgoing emitted light caused by coupling to the SPR.^[3] Furthermore, considering the dimensions of the spherical nanoparticle, surface enhanced photoluminescence can be established from the transfer of energy between the excited fluorophore and the metallic nanoparticle, otherwise known as FRET.

CHAPTER 3. EXPERIMENTAL PROCEDURE AND RESULTS

3.1 Sample Preparation

This chapter describes the analytical techniques used to create and characterize the nanoparticle-dye molecule system used in this research. The nanoparticle-dye system studied was a mixture of nanoparticles and dye molecules in aqueous medium rather than a mixture of nanoparticles and dye molecules cast into a thin film or an aqueous solution of dye molecules in contact with a thin film composed of nanoparticles, as studied by others.^[28-30] Several combinations of nanoparticle-dye solutions were created to determine the most stable and most optically efficient solution.

3.1.1 Nanoparticle Synthesis

Metallic nanoparticles were synthesized by a well-developed method^[7] with the exception of using de-ionized water as the solvent instead of TOAB. The aqueous solutions were created in a beaker and transferred to quartz cuvettes which were used to decrease the amount of UV light absorbed into the cuvette for sample testing. Gold nanoparticles were synthesized using the reduction of hydrogen tetrachloroaurate (III) (HAuCl_4 , 99%).^[7] The primary synthesis solution contained the HAuCl_4 along with sodium carbonate (Na_2CO_3) to start the activation of the gold. These two components were combined in a 150ml beaker of de-ionized water, used to create a stock solution, and stored in a dark location for 24-48 hours to allow the reaction to progress to completion. This could be detected by visual examination of the solution as the initially yellow solution converted to a clear solution upon the completion of the combination. Just prior to creating a sample of the nanoparticles, the second solution is made. This solution consists of sodium borohydride (NaBH_4) and de-ionized water. The second solution, when combined with the first solution, caused the reduction of the gold to create gold colloids; varying the concentration of sodium borohydride to water varied the amount and size of colloids synthesized.

A similar method is used to create the silver colloids. Two solutions are also necessary to complete the synthesis of silver particles; the second solution is the same in both processes. The source of silver for the reaction was a dilute solution of silver nitrate (AgNO_3).^[12] This solution is also stored overnight to allow complete mixing of the concentrated silver nitrate with de-ionized

water. Once again, the sodium borohydride solution is used as a reducer and stabilizer to create the silver nanoparticles.

In some of the synthesis runs to form gold colloids, the creation of silica nucleation sites was used to stabilize high concentrations of the gold nanoparticles as well as prevent aggregation.^[37] In this case, silicon dioxide colloids (SiO_2), already suspended in an aqueous solution, were combined with tin chloride ($\text{SnCl}_2 \cdot 2\text{H}_2\text{O}$); the tin chloride is used to activate the surface of the silicon dioxide nanoparticles. The solution was then centrifuged for 2 hours, rinsed with de-ionized water, and repeated four times to remove the excess tin (Sn^{2+}) molecules from the surface of the particles. Once completed, the solution of Sn-sensitive silicon dioxide nanoparticles was mixed with the primary gold solution (HAuCl_4 and Na_2CO_3) and stirred rapidly; the solution was placed on a low temperature heater to aid in faster and more complete synthesis. The final stage of synthesis requires the reduction of the gold using formaldehyde (37%).

3.1.2. Dye Solution Synthesis

Two dyes were used in the experiment to test the energy exchange capabilities of the nanoparticles. The first dye used was chromoionophore I (5294); this dye was considered to be a weak fluorophore. As it is used extensively with thin films to detect potassium via changes in its fluorescence, an application that will be discussed in detail later, improvement in the fluorescence efficiency was desired. Thus, characterization of chromoionophore I in solution with gold and silver nanoparticles was performed. The second dye used was sulforhodamine 101. Previous research had used a similar dye, rhodamine B, to interact and study nanoparticles.^[2] Sulforhodamine has similar properties to rhodamine B and was readily available commercially. Dilute solutions of the dyes dissolved in de-ionized water were made with similar concentrations of each dye solution used in combination with the synthesized metallic nanoparticles.

3.2 Optical Characterization Techniques

This section will discuss the methods used to determine the interaction of the nanoparticles with the dye molecules, show the requisite data, and compare the data between the three types of nanoparticle-dye solutions described in the previous section.

3.2.1. Photoluminescence Excitation Spectroscopy

Photoluminescence excitation is a method used to determine the peak pump intensity needed to excite the peak photoluminescence (PL) from a film or solution as well as locate additional excitation wavelengths. In this experiment, the photoluminescence (PL) signal was obtained by exciting the dye with relatively monochromatic light. This excitation source was formed by coupling the optical output of a tungsten lamp through a single monochromator, resulting in a wavelength-tunable source. The PL intensity within a specified wavelength range was recorded as the excitation energy was scanned. Measurements were taken for dye-only solutions, dye-gold nanoparticle solutions, dye-silver nanoparticle solutions, silver-only solutions, and gold-only solutions for comparison. A Jobin Yvon Spex® 1680 and dual monochromator spectroscopy system were used in the experiment.

3.2.2. Fluorescence Spectroscopy

The samples were then characterized by measuring the PL signal obtained when exciting the dye using an excitation wavelength identified from the PLE experiments. Based on the results of the PLE data or absorption data (discussed later), a specific pump wavelength is set and the corresponding fluorescence intensity is measured. The pump wavelength is used to excite the sample by allowing the absorption of a photon by the sample. The absorption elevates the molecule from ground state to a vibrational state. As the excited molecule/molecules collide, the vibrational energy decreases until it reaches its lowest vibrational state. Once the molecule leaves this final vibrational state and returns to a ground state level, the photon may be emitted though light is not always generated by the decay of the excited molecule back to its ground state. If a photon is emitted, however, it may have a different energy than when it was first absorbed, thereby creating different frequencies. Fluorescence spectroscopy records the behavior of the optical transitions, though not the number or magnitude of intermediate transitions, by detecting the varying frequencies of the emitted light (PL). The plot of the fluorescence is given by the intensity versus the wavelength. In several cases, the PL intensity was too high and neutral density filters were used to prevent the saturation of the photomultiplier tube.

3.2.3. Absorption Spectroscopy

Gold, silver, and other noble metal nanoparticles display a strong visible ultraviolet absorption band unlike their bulk material counterparts. This absorption band becomes evident in with the onset, or induction, of the surface plasmon resonance as described in Chapter 1. During this process, the incident light is resonant with the oscillations of the conduction electrons from the metallic nanoparticles. Observations of this phenomenon result in potentially resonant Rayleigh scattering (described in Chapter 2), absorption at specific wavelengths (measured by absorption spectroscopy), and an enhancement of the electromagnetic field near the surface of the metallic nanoparticle; note that the latter enhancement affects other parameters including energy transfer. In addition, the Mie theory in Chapter 2 also highlights the effects of absorption and extinction coefficients of the metallic nanoparticles in long wavelengths. Absorption data is also, therefore, indicative of the size and shape of nanoparticles. Each element has a specific or characteristic absorption intensity based on the absorption of a photon of light by the dye or nanoparticle in the system. The excitation energy can be determined by the wavelength of the incident photon as mentioned previously. Though the intensity of the absorption may not vary based solely on the material properties, the absorbance of a material has been shown to be proportional to the molar concentration of the absorbing molecule as well as the thickness of the sample (Beer's law). Likewise, the medium surrounding the nanoparticles, the size and shape of the nanoparticles, the dielectric constant of the metallic nanoparticle, and the actual absorption contribute to the extinction coefficient of the sample itself. A simplified version of the Mie theory equation given in Chapter 2 describes this relationship:

$$E(\lambda) = \frac{24\pi N_A a^3 \epsilon_m^{3/2}}{\lambda \ln(10)} \left[\frac{\epsilon_i}{(\epsilon_r + \chi \epsilon_m)^2 + \epsilon_i^2} \right] \quad (1)$$

$E(\lambda)$ is the extinction coefficient, N_A is the density of the nanoparticles, a is the radius of the nanoparticle, ϵ_m is the dielectric constant of the surrounding medium, λ is the absorption wavelength, ϵ_i is the imaginary component of the dielectric constant for the metallic nanoparticle, ϵ_r is the real component of the dielectric constant of the metallic nanoparticle, and χ is the aspect ratio of the nanoparticle; since we are using spherical nanoparticles, χ is equal to two.^[38]

Therefore, the extinction coefficient contributes significantly to the overall absorption based on Mie's theory. The absorption spectra, consequently, is the plot of the absorbance versus absorption wavelength. Again, measurements were taken for dye-only solutions, dye-gold nanoparticle

solutions, dye-silver nanoparticle solutions, silver-only solutions, and gold-only solutions for comparison. Measurements were taken using the Shimadzu UV-VIS spectrometer and scanning over a range of 300-800 nm.

3.2.4. Transmission Electron Microscopy (TEM)

Transmission electron microscopes are used to enhance and enlarge images of biological, chemical, and other miniature specimen that may be invisible to the naked eye. These images are created by focusing an electron beam onto the specimen, causing an enlarged representation to appear on film or detected by a camera. Though the TEM imaging process is much more complex than described in this document, we use a simplified description since TEM was used for size and spacing verification purposes only. For our samples, TEM was used to detect the aggregation of particles as a means of supporting absorption and PLE data. In addition, the TEM images provided a visual means of documenting the size and shape of the nanoparticles synthesized.

3.3 Experimental Results

This section begins with a comparison of the absorption, fluorescence, and photoluminescence excitation data of the nanoparticle-only systems. In addition, data was collected on a commercially produced solution of 20nm-sized nanoparticles and compared to the synthesized particles described above. Once this comparison was made, and verified through TEM, analysis of the data was made to correlate theory to the practical data. It should be noted that prior to any data collection, each piece of equipment was aligned according to documented procedure to ensure reproducible results.

3.3.1. Sulforhodamine 101 Characterization and Analysis

A sample of sulforhodamine 101 (S101) was dissolved in de-ionized water to obtain a molar concentration of 3.95×10^{-6} M. The sample color was light wine red. The sample solutions had a final volume of 9ml the following data is based on a diluted S101 solution (1ml S101 solution mentioned previously and 8 ml of de-ionized water). The resulting solution was a pale pink color. In Figure 4, notice that the PLE data identifies optimal excitation wavelengths of 550nm and 588nm for the PL wavelength of 609 nm for this sample. There was a return of the pump wavelength in both cases. Based on the data, we expect to have substantial fluorescence intensity when we pump at 588nm. Upon exciting the sample at 588 nm, we saw significant

fluorescence at 605nm; see Figure 5. Subsequent data was collected for the excitation at 550nm as shown in Figure 6. Notice that, although substantial fluorescence intensity is observed at 605nm again, the intensity is not as strong as the previous excitation wavelength of 588nm. This indicates that, for the diluted S101 sample, optimal excitation for maximum fluorescence in the 600nm range is 588nm.

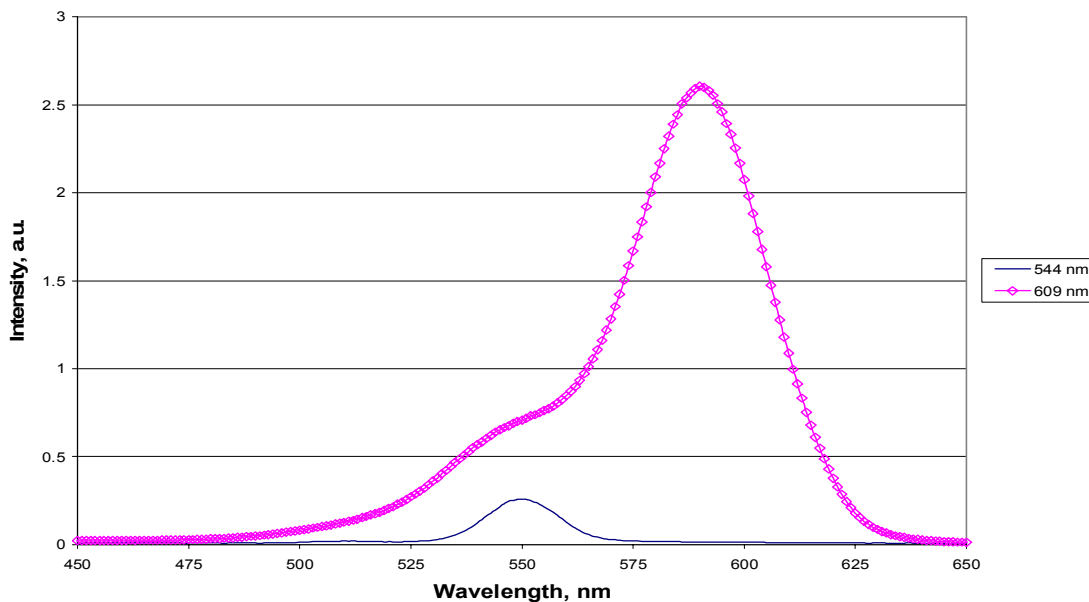


Figure 4. PLE data for 1ml of S101 diluted in 8ml of DI water.

Absorption data was also collected for the sample (Figure 7). Both the 550nm and 588nm absorption peaks were also observed for the sample, verifying the appropriate excitation energies required to provide maximum quantum efficiency and fluorescence.

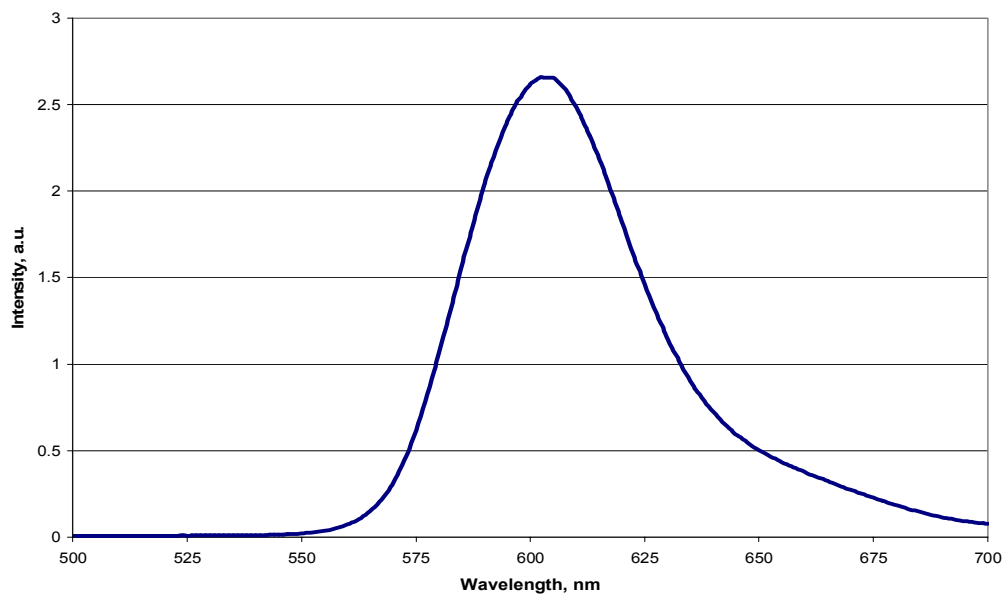


Figure 5. Photoluminescence data for 1ml of S101 diluted in 8ml of DI water excited at 588nm. Significant fluorescence is noted at longer wavelengths than 605nm.

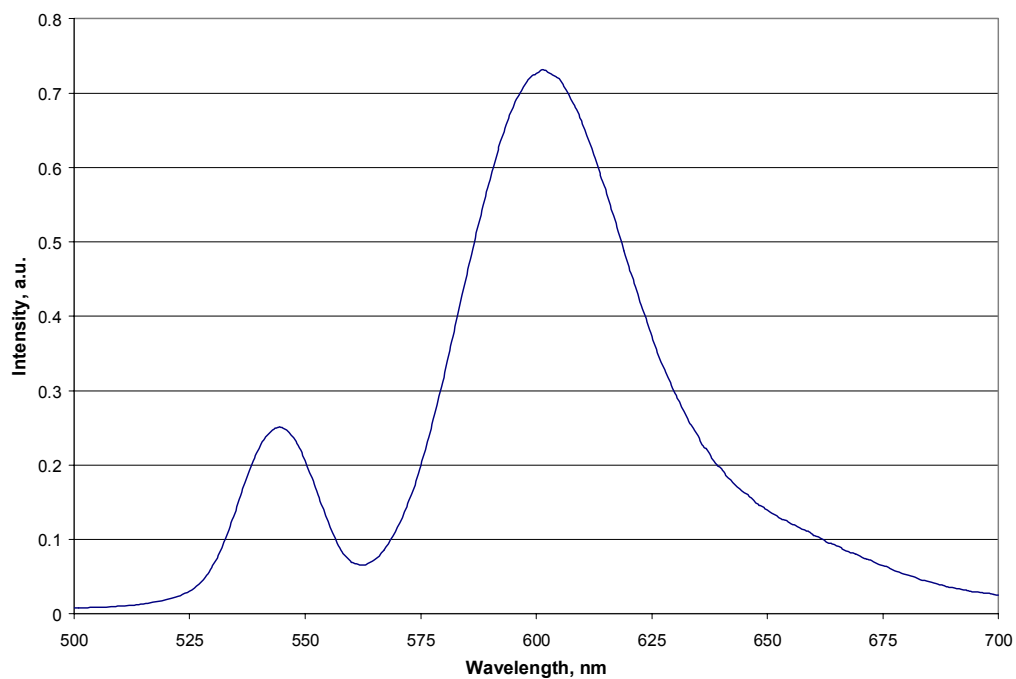


Figure 6. PL data collected when exciting the 1ml of S101 diluted in 8ml of DI water at 550nm. Though significant fluorescence is shown at 605nm, the intensity of the fluorescence is not as substantial as the previous data collected at the excitation of 588nm.

3.3.2. Gold Nanoparticle Characterization and Analysis

Similar tests were performed on samples of synthesized gold nanoparticles. This data provided information on baseline absorption data for 20nm gold nanoparticles. Prior documentation noted that the maximum absorption for 2-5nm gold nanoparticles was observed at 517nm^[14], however a comparison of a known sample of 20nm gold nanoparticles with our synthesized particles indicated that the absorption peak for 20nm gold nanoparticles is in the range of 521-530nm. We should note that fluorescence data was not collected on gold-only or silver-only samples since the data consisted, primarily, of scattered pump wavelengths. The synthesized 20nm gold nanoparticles were wine red in color, corresponding to Mie's theory of gold nanoparticles noted earlier in this document. Based on the solution color and the absorption data, the particle size was verified. Figures 7 and 8 give the comparison of a known sample of 20nm nanoparticles with the synthesized nanoparticles we generated. TEM images, not shown, of the two samples were also used for size verification.

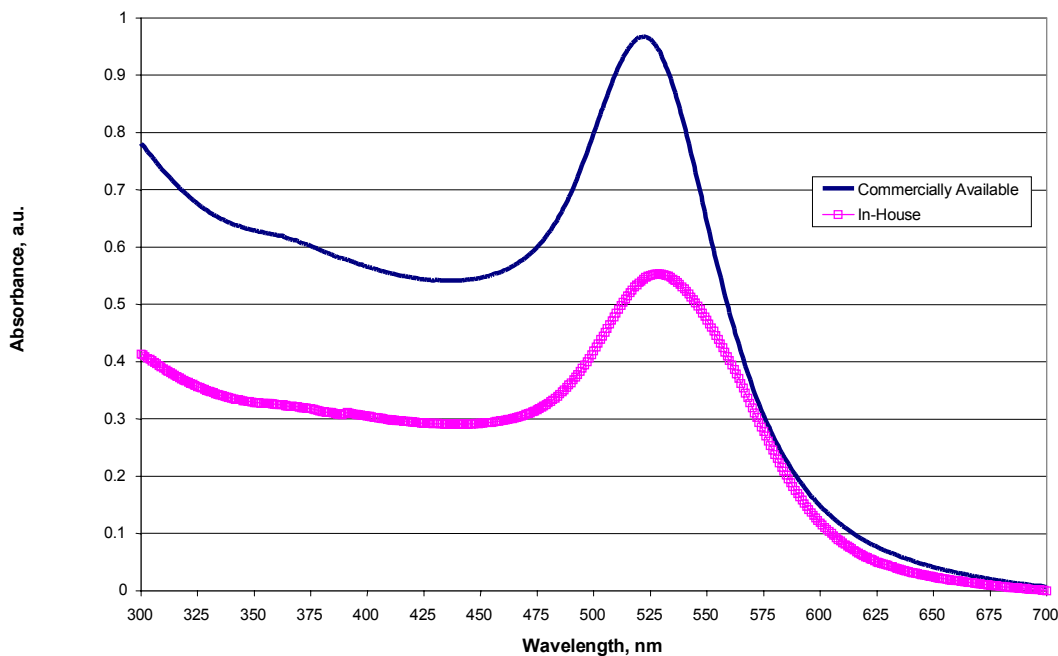


Figure 7. Absorption comparison of known-sized gold nanoparticles and the generated sample.

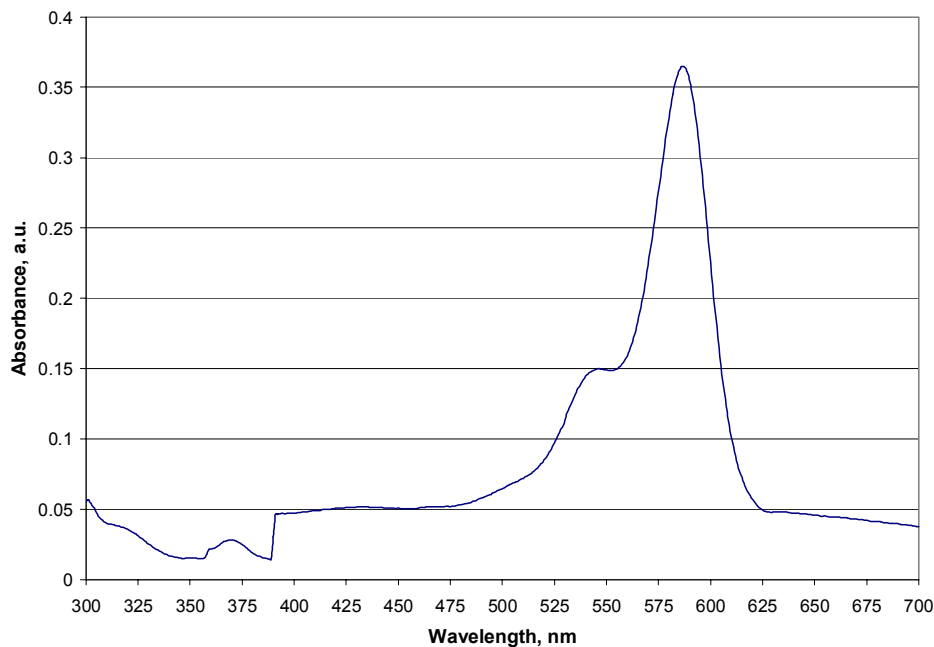


Figure 8. Absorption data obtained for diluted S101 sample. Notice the absorption peaks at 550nm and 588nm. This indicates that maximum absorption occurs at these wavelengths. Data coincides with both the PLE and the PL data collected previously.

3.3.3. Gold-S101 Solution Measurements and Characterization

Gold nanoparticles were combined with the S101 solution described previously. A matrix of solutions was created by keeping the concentration of S101 constant and varying the amount of nanoparticle solution and de-ionized water added to obtain a final sample volume of 9ml. Holding the S101 concentration constant at 1ml and varying the concentration of water and gold nanoparticles, we observed that the absorption peak of the solution is dominated by the gold concentration (Figure 9). Because of its behavior, when fluorescence tests were performed, the sample showed very little fluorescence (not shown).

When the concentration of S101 was increased to 3ml, the absorption data still indicated that the behavior of the sample solution reflects the same absorption behavior as the gold-only solution (Figure 10). However, when compared to the 1ml S101 samples, there is a distinct increase in the absorbance of the system.

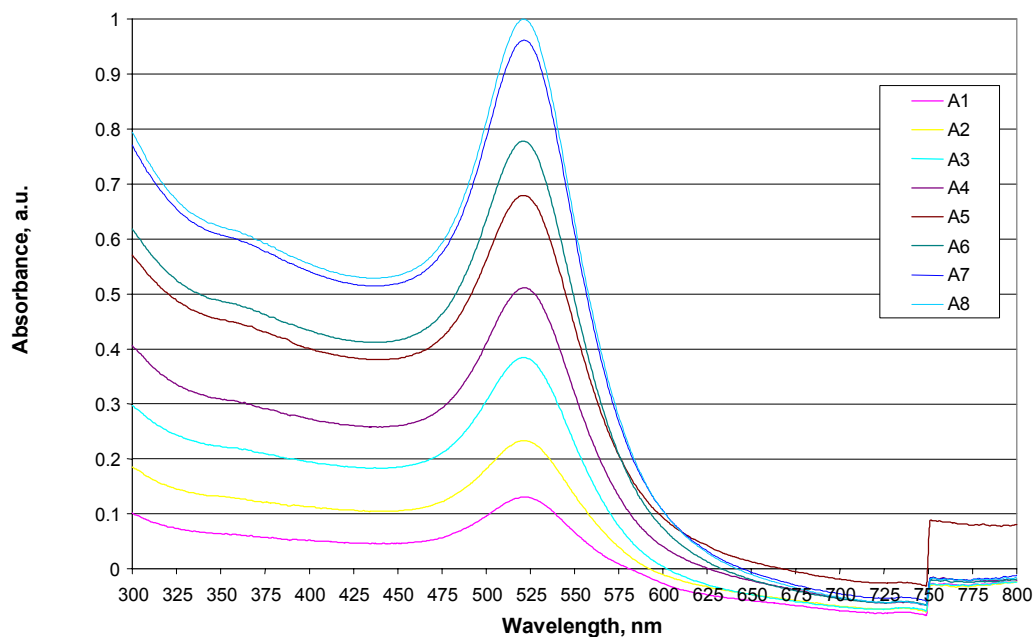


Figure 9. Absorption data for 1ml S101 solution with varied concentrations of gold nanoparticles. The legend details the concentration of gold nanoparticles (i.e. A1=1ml of solution containing gold nanoparticles. A2 = 2ml of the gold colloid solution, etc.) for a total sample volume of 9ml. Note that the data was normalized.

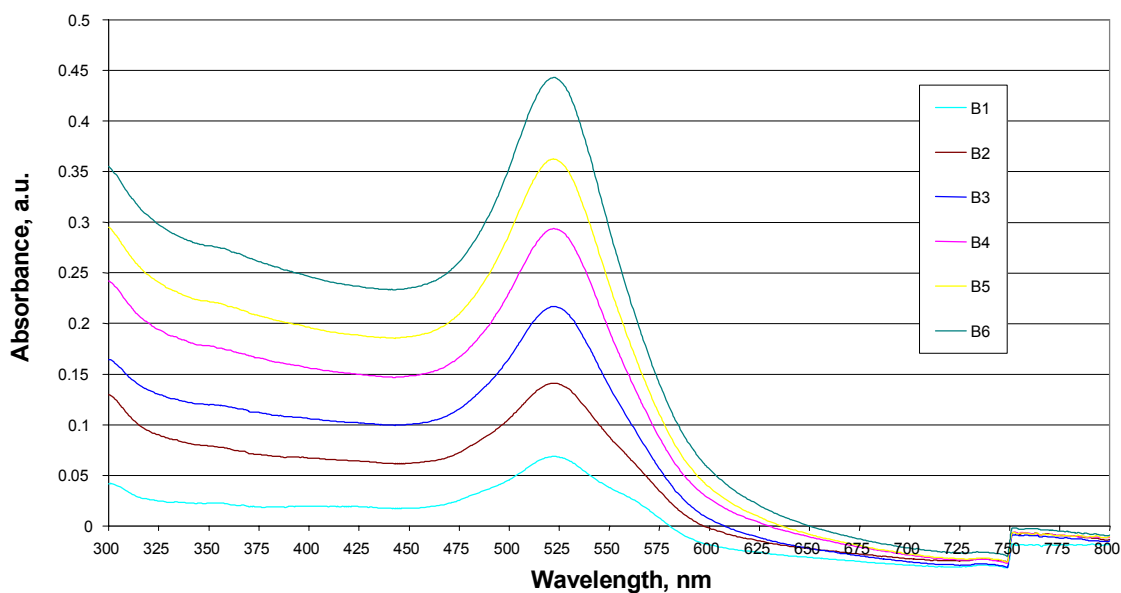


Figure 10. Absorption data of gold/3ml S101 solution. Though there was not a shift in the data, as expected, there is an increase in the absorbance. Note that the total sample solution is 9ml and the legend indicates the amount of nanoparticles present in the solution (i.e. B1= 1ml gold nanoparticles).

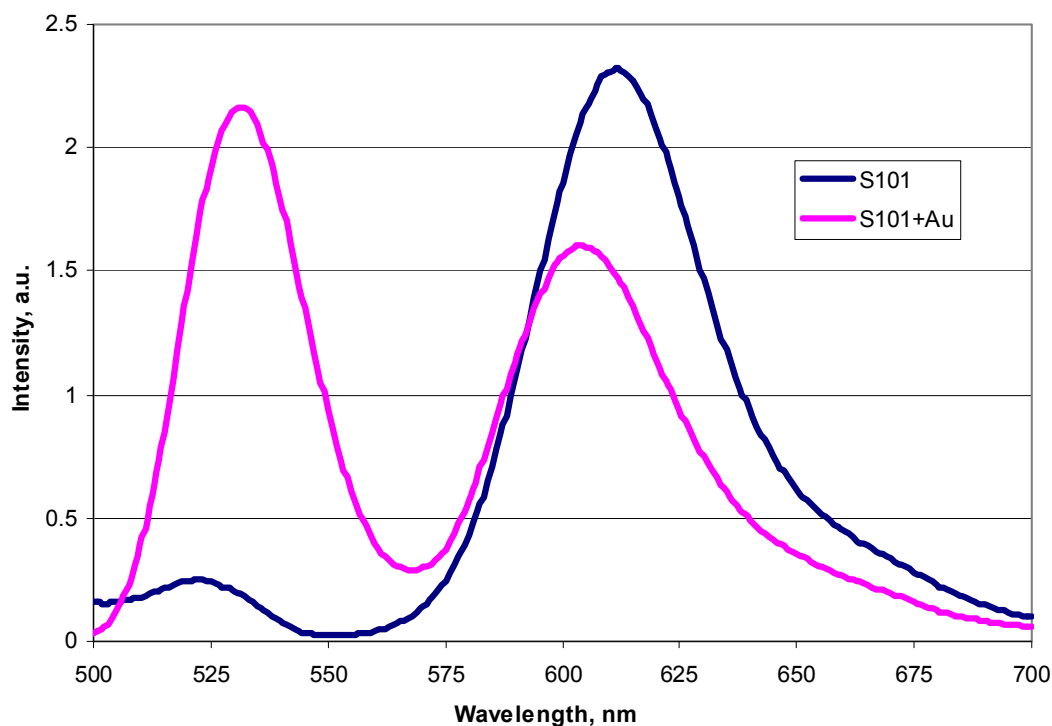


Figure 11. PL data for gold-dye system. Note the excitation wavelength is 544nm and that the peak at 609nm decreases with the addition of the gold nanoparticles.

3.3.4. Gold-Dye Analysis

Figures 9 and 10 display the absorption spectra of the gold-dye system with 1ml of dye and 3ml of dye, respectively. We observed that as the gold nanoparticle concentration increased, the absorbance also increased. In addition, we note that the absorption peak of the S101 and the absorption peak of the gold overlap at approximately 525nm and, therefore, is indistinguishable in both sets of data. We also observed that there is a slight peak around 544nm in Figure 10. We used this data to test for fluorescence at 609nm.

Figure 11 is the fluorescence spectra collected for the 1ml S101 solution. Based on the data collected in Figure 9 and 10, we excited the sample at 544nm. We observed that a significant fluorescence peak exists at 609nm, however the fluorescence corresponding to the dye-nanoparticle solution seems to decrease or quench. In fact, the abundance of gold nanoparticles compared to the concentration of the dye caused quenching of any detectable fluorescence. In

addition, the secondary peaks found at 525nm are indicative of the scattering of the excitation wavelength and do not relate to the overall fluorescence of the system.

3.3.5. Silver Nanoparticle Characterization

Data was collected on commercially available and in-house synthesized samples of silver nanoparticles. Observations found that the maximum absorption peak is located in the range of 400-410nm. Previous documentation on smaller nanoparticles indicated an absorption peak at 380nm.^[30] The nanoparticles synthesized in-house became unstable within 2-3 days of experimental procedures and reverted back to their previously clear state, described in Section 3.1.1. Generation of new samples before characterizing the various dye-silver nanoparticle solutions was time consuming so the commercially available 20nm silver nanoparticles were used for the remainder of the testing. Figure 12 shows the absorption comparison between the known and generated sample.

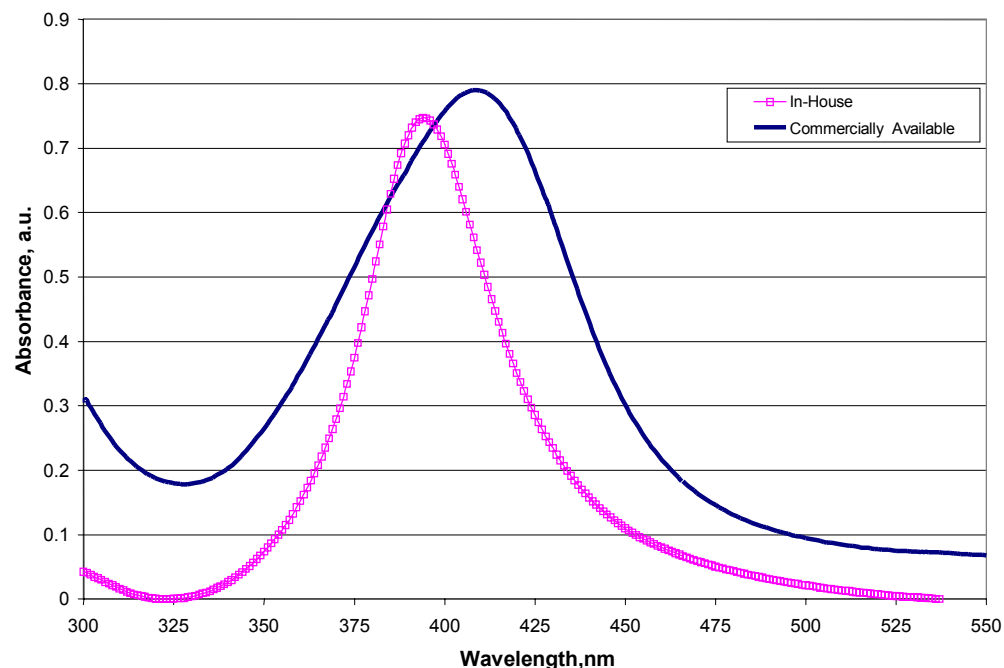


Figure 12. Comparison of absorption data for 20nm silver nanoparticles. Note that the in-house nanoparticles had better monodispersity than the commercially available sample. However due to the lack of aqueous stability, we chose to use the commercially available nanoparticles.

3.3.6. Silver-S101 Measurements and Characterization

Similar tests were performed for the silver nanoparticles with both 1ml and 3 ml solutions of the S101 solutions. We should note that we did perform tests on solutions of 2ml of S101. These measurements, however, showed no significant changes to the overall system (i.e. absorbance shifts or increases). Tests of the silver-1ml dye systems showed significant results as compared to the data collected in the gold-dye systems.

3.3.7. Silver-Dye Analysis

Figure 13 shows the absorption spectra for the 1ml S101-silver nanoparticle system. We observed that, in addition to the absorption peak of the silver located at 410nm, a smaller absorption peak is located at 580nm. We observed a similar peak for the S101 only sample (Figure 8). The absorbance due to the silver nanoparticles is substantially greater than that of the S101 peak. The two distinctive peaks indicate an absence of interaction amongst the silver and dye particles; the two peaks did not shift or increase in absorbance when combined, according to the measurement. It should be noted that the peak shown at 580nm was not visible in the gold nanoparticle-dye system; we assume that since the SPR peak overlaps with the absorption peak of the gold nanoparticles, the distinction between the two sources is indecipherable.

Figure 14 shows the fluorescence data taken for the silver-dye system. Note that there is significant intensity at the 588nm mark, once again, to achieve maximum fluorescence at 609nm. In addition, we observed the reappearance of the 550nm secondary peak. Based on this information, we performed the fluorescence tests and pumped (excited) our sample at 588nm. Figure 15 shows the results of this experiment in addition to additional excitation wavelengths of 514nm and 544nm, both derived from the PLE data of the dye only system and the nanoparticle only system, beyond the surface plasmon resonances they displayed. We observed that though there is fluorescence at 609nm with all of the excitation wavelengths, there was significant fluorescence for the excitation wavelength of 588nm. We also noted that the secondary peaks of both the 514nm and 544nm were deemed the scattering of the excitation wavelength and held no bearing on the peaks found at 609nm.

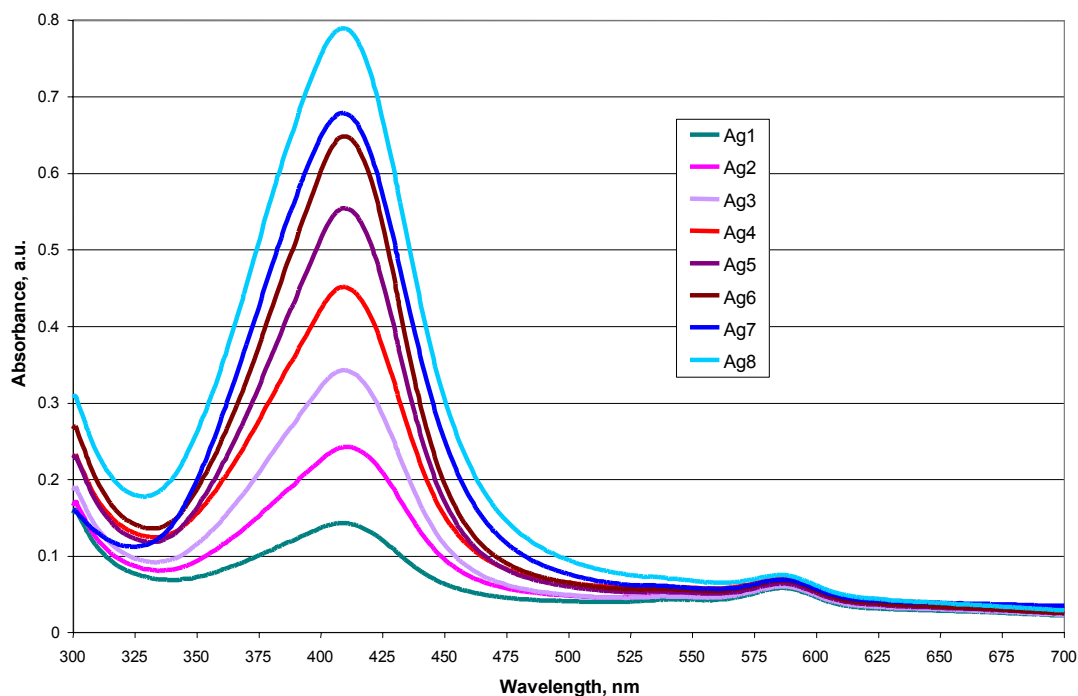


Figure 13. Absorption data for the 1ml S101-silver nanoparticle system. Note the secondary peak located at 588nm. This peak is similar to the absorption peak for the S101-only solution. The peak for the silver nanoparticles (414nm) seems to increase in absorbance as the concentration of silver increases.

In addition, our experiments observed that the significant fluorescence achieved in the dye-silver nanoparticle system was not repeated in the dye-gold nanoparticle experiments. Instead, we note that a comparison of Figures 11 and 14 shows that the gold-dye system quenches its fluorescence at 609nm whereas the silver-dye system enhances the fluorescence. We determined that the quenching was due to reverse FRET; this means that the acceptor molecule was exchanging energy with the donor instead of vice versa. Energy transfer is occurring but not by the means dictated by the Förster-Dexter theory (i.e. the Forster distance, the back transfer of the emission of the donor molecule, and the orientation of the dipoles).

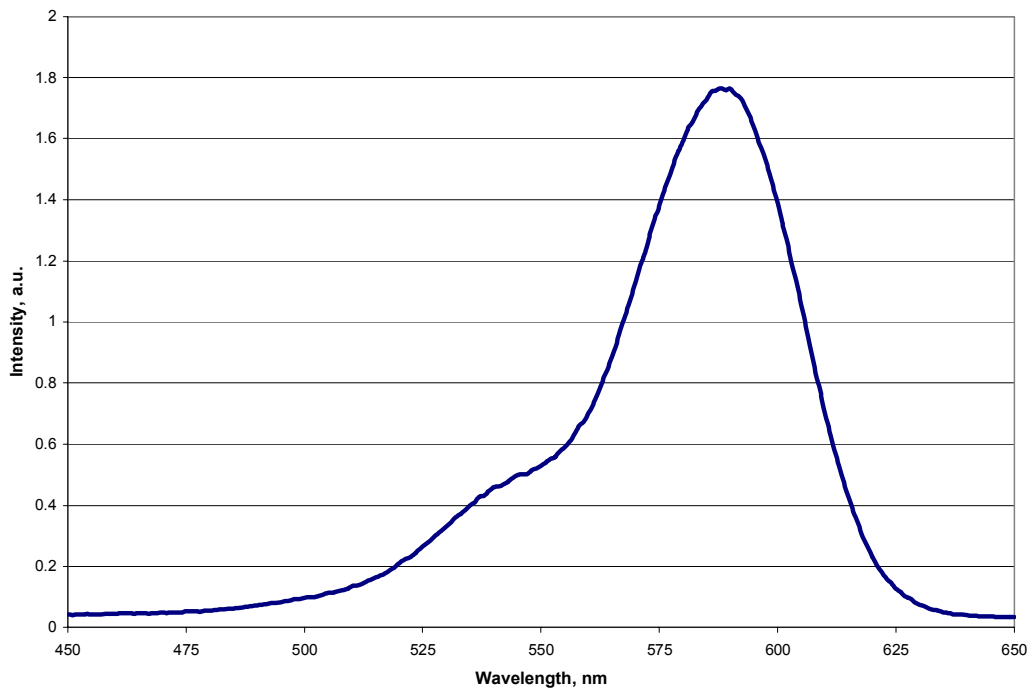


Figure 14. PLE data for the dye-silver nanoparticle solution with 1ml of S101 and 2 ml of silver nanoparticles. Notice that the maximum excitation peak is still found at 588nm with a secondary peak at approximately 550nm for fluorescence at 609nm.

The enhancement shown in the silver-dye system is due to resonance energy transfer initiated by Raman scattering. We note that the incident wavelength energy indicated is not the same energy that exits the sample (i.e. the fluorescence of the system). In addition, we also expect that the electric field interaction from the incident light to the nanoparticle has an effect on the enhancement as well. The overall response is best documented by Mie's theory of scattering.

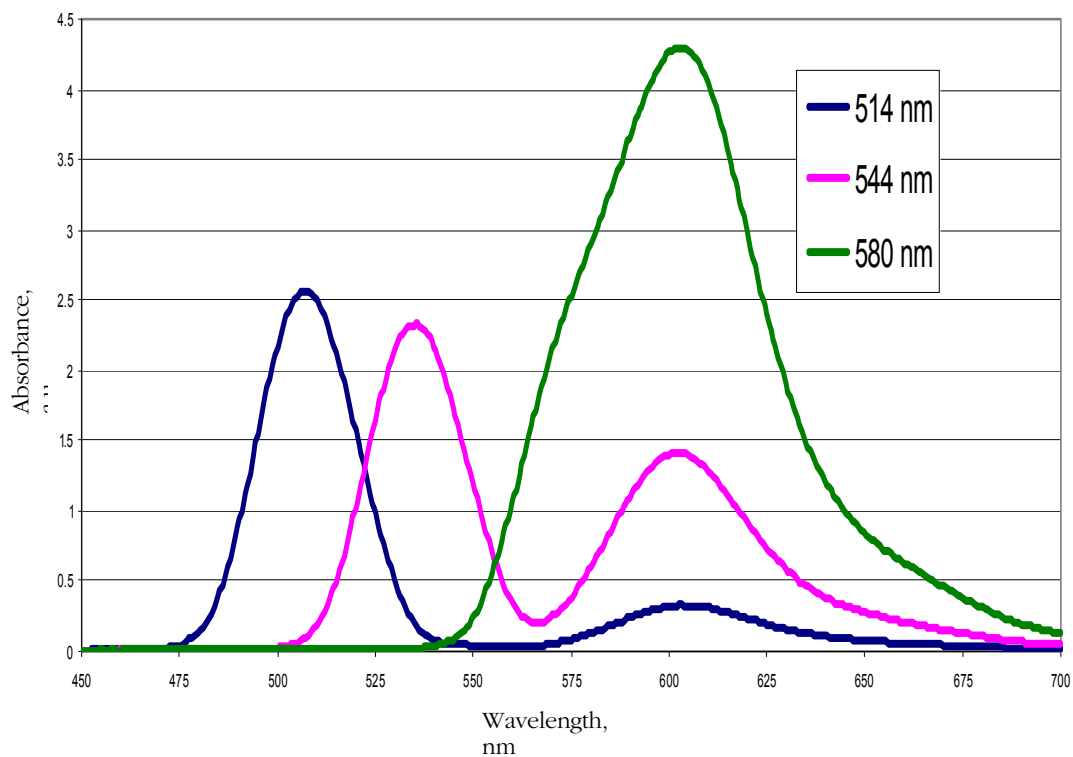


Figure 15. PL data for the silver-dye sample. Notice that excitation at 580nm gives significant fluorescence at 609nm. It should be noted that for the excitation wavelengths of 514nm and 544nm (determined from PLE data), the peaks at those wavelengths indicate scattering of the excitation wavelength.

CHAPTER 4. CONCLUSIONS AND FUTURE WORK

The results described in Chapter 3 provide a progressive step in understanding the behavior of silver and gold nanoparticles in a fluorescence dye (fluorophore) system. We have noted several theories about the excitation of surface plasmons in Chapters 1 and 2 and described the reaction to these excitation mechanisms. Building off of the principle theory of light scattering (Rayleigh scattering), Mie described a system that considered the affects of the surrounding media with the incident light and how its response affected the response of the excited molecule. Raman further exploited this theory by observing the change in frequency of the exiting radiation from the sample. Finally, Förster and Dexter combined these theories to describe the energy transfer from the excited donor to the acceptor. Our system, described extensively, has displayed properties of all of these theories of excitation.

Chapter 1 described the generation of the surface plasmon resonance from thin films to spherical nanoparticles. The maximum surface plasmon resonance is achieved when the incident light frequency is equivalent to the oscillation of the free electrons found on a metallic surface. For nanoparticles, surface plasmon resonance is considered localized because the resonance condition is found on its surface and does not require a specific geometric setup to excite the surface plasmons. Conversely, thin films of nanoparticles require the Kretschmann geometry described and shown in Chapter 2. Achieving maximum surface plasmon resonance allows for the enhancement or quenching of a signal since metallic nanoparticles absorb and transfer an abundance of energy.

We began our research with the intent of developing an optical sensor that has optimized the surface plasmon resonance to amplify a signal within the sensor. We soon discovered that understanding the interactions between the nanoparticle and the dye was significant before incorporating it into a system with a variety of other components. We chose a dye, similar in characteristics as the dye we wish to use in the sensor, to study the effects. (Sulforhodamine 101 is a strongly fluorescent dye that shares the characteristics of the weakly fluorescent chromoionophore 1.) After noting that previous research^[8, 28-30] used thin films, we decided to investigate the colloidal system instead since the final system will combine the nanoparticles in the sensor itself.

As indicated in our analysis, we observed that the addition of metallic nanoparticles, could either quench or enhance the fluorescence of the signal. In the case of gold nanoparticles, we observed significant quenching of the fluorescence at the all excitation wavelengths while the silver nanoparticles displayed characteristics of enhancement. In addition, we believe that incorporating the chromoionophore 1 into the system, we expect to see even more fluorescence enhancement from the silver-dye system since the dye is weakly fluorescent and the absorption spectra indicates the strong influence of the silver.

For the future, we expect the previous research to be expanded and explored further. Understanding the complete interaction of nanoparticles and dye allows the ability and flexibility of using these systems in inorganic and organic devices. For our specific sensory device, we expect to explore the characteristics of the chromoionophore 1-nanoparticle system and document the interaction using surface enhanced Raman spectroscopy, mentioned in Chapter 3. This analysis provides relevant information about the distances between the fluorophore molecule and the metallic surface, a key to understanding the transfer of energy via FRET. This was a limitation in our research since TEM images cannot display organic molecules. Another mechanisms for determining the proximity of the dye to the metal is laser scattering; like spectroscopy methods described previously, specific systems scatter light in a characteristic manner and additional influences affect this scattering. In addition, these analysis techniques could disclose additional optical characteristics of the system and open the door to completely understanding the optical properties of dye-nanoparticle systems.

BIBLIOGRAPHY

- [1] Y. Xu, K. Meehan, B.J. Love, N. G. Love, and K. A. Linares, "pH Dependent Changes in the Optical Properties of Surface Modified Gold Nanoparticles Using Bovine Serum Albumin Coating," *Proc. Nanotechnology 2004*, **1**, 15-18, 2004.
- [2] S. Franzen, Jacob C. W. Folmer, Wilhelm R. Glomm, and Ryan O'Neal, "Optical Properties of Dye Molecules Adsorbed on Single Gold and Silver Nanoparticles," *Journal of Physical Chemistry, A*, **106**, (28), 6533-6540, 2002.
- [3] S. Link, Mostafa A. El-Sayed, "Shape and size dependence of radiative, non-radiative and photothermal properties of gold nanocrystals," *Int. Reviews in Physical Chemistry*, **19**, (3), 409-453, 2000.
- [4] P. N. Prasad, *Nanophotonics*. Hoboken: John Wiley and Sons, Inc., 2004.
- [5] L. He, E. Smith, M. J. Natan, and C. D. Keating, "The Distance-Dependence of Colloidal Au-Amplified Surface Plasmon Resonance," *Journal of Physical Chemistry, B*, **108**, (30), 10973-10980, 2004.
- [6] I. Vargas-Baca, Andrew P. Brown, Mark P. Andrews, Tigran Galstian, Yuejun Li, Hojatollah Vali, and Mark G. Kuzyk "Linear and nonlinear optical responses of a dye anchored to gold nanoparticles dispersed in liquid and polymeric matrixes," *Canadian Journal of Chemistry*, **80**, (11), 1625-1633, 2002.
- [7] P. V. Kamat, "Photophysical, Photochemical and Photocatalytic Aspects of Metal Nanoparticles," *Journal of Physical Chemistry, B*, **106**, 7729-7744, 2002.
- [8] J. R. Lakowicz, "Radiative decay engineering: 3. Surface plasmon-coupled directional emission," *Analytical Biochemistry*, **324**, (2), 153-169, 2004.
- [9] C. Mak, A. Pern, T. Yan, B.D. Yu, "Surface Plasmon Microscopy," University of California, Report 2004, http://alpern.bol.ucla.edu/projects/284/spm_paper.pdf.
- [10] U. Kreibig and Michael Vollmer, *Optical Properties of Metal Clusters*, Springer Series in Materials Science, vol. 25, Berlin: Springer-Verlag, 1995.
- [11] J. I. Gerstein, Abraham Nitzan, "Accelerated Energy Transfer Between Molecules Near a Solid Particle," *Chemical Physics Letters*, **104**, (1), 31-37, 1984.
- [12] T. Pal, N.R. Jana, and T. Sau, "Nanoparticle Induced Fluorescence Quenching," *Radiative Physical Chemistry*, **49**, (1), 127-130, 1997.
- [13] M.R. Shortreed, S.Dourado, and R. Kopelmann, "Development of a fluorescent optical potassium-selective ion sensor with ratiometric response for intracellular applications," *Sensors and Actuators B*, **38**,(1-3), 8-12, 1997.
- [14] A. Yu, Z. Liang, J. Cho, and F. Caruso, "Nanostructured Electrochemical Sensor Based on Dense Gold Nanoparticle Films," *Nano Letters*, **3**, (9), 1203-1207, 2003.
- [15] L. Burgess, "Absorption-based sensors," *Sensors and Actuators B*, **29**, (1-3), 10-15, 1995.
- [16] C.B. Bott and N.G. Love, "Investigating a mechanistic cause for activated sludge deflocculation in response to shock loads of toxic electrophilic chemicals," *Water Environment Research*, **74**, (2), 306-315, 2002.
- [17] H. He, H. Li, G. Mohr, B. Kovacs, T. Werner, and O. Wolbeis, "Novel type of ion-selective fluorsensor based on the inner filter effect: an optode for potassium," *Analytical Chemistry*, **63**, (1), 123-127, 1993.
- [18] D. Long, *The Raman Effect: A Unified Treatment of the Theory of Raman Scattering by Molecules*, West Sussex: John Wiley & Sons, Ltd., 2002.

- [19] Wikipedia contributors (2006). Raman scattering. *Wikipedia, The Free Encyclopedia*. Retrieved 22:50, March 11, 2006 from http://en.wikipedia.org/w/index.php?title=Raman_scattering&oldid=40383588
- [20] G. Mie, "Contributions on the optics of turbid media, particularly colloidal metal solutions," Translation # 79.21946 (Sandia National Laboratory), *Annalen der Physik*, **25**, (3), 377-445, 1908.
- [21] J.D. Dow, "Resonance Energy Transfer in Condensed Media from a Many-Particle Viewpoint," *Physical Review*, **174**, (3), 963-976, 1968.
- [22] H.C. Cheung, "Resonance Energy Transfer," *Topics in Fluorescence Spectroscopy, Volume 2: Principles*, ed. J.R. Lakowicz. New York: Plenum Press, 1991.
- [23] S. H. Lin, W.Z. Xiao, and W. Dietz, "Generalized Forster-Dexter theory of photoinduced intramolecular energy transfer," *Physical Review E*, **47**, (5), 3698-3706, 1993.
- [24] P.R. Selvin, "The renaissance of fluorescence resonance energy transfer," Review Article, *Nature*, **7**, (9), 730-734, 2000.
- [25] T. Ha, T. Enderle, D.F. Ogletree, D.S. Chemla, P.R. Selvin, and S. Weiss, "Probing the interaction between two single molecules: Fluorescence resonance energy transfer between a single donor and a single acceptor," *Proc. Natl. Acad. Sci. USA*, **93**, (13), 6264-6268, 1996.
- [26] R.M. Clegg, *Fluorescence Imaging Spectroscopy and Microscopy*, ed. X.F. Wang and B. Herman. Chemical Analysis Series, Volume 2, New York: John Wiley & Sons, 1996.
- [27] W. L. Barnes, "Fluorescence near interfaces: the role of photonic mode density," *Journal of Modern Optics*, **45**, (4), 661-699, 1998.
- [28] J.R. Lakowicz, "Radiative Decay Engineering: Biophysical and Biomedical Applications," *Analytical Biochemistry*, **298**, (3), 1-24, 2001.
- [29] J.R. Lakowicz, "Radiative Decay Engineering: the role of photonic mode density in biotechnology," *J. Phys. D: Appl. Phys.*, **36**, 14, R240-R249, 2003.
- [30] J.R. Lakowicz, "Radiative Decay Engineering: 2. Effects of Silver Island Films on Fluorescence Intensity, Lifetimes, and Resonance Energy Transfer," *Analytical Biochemistry*, **301**, (2), 261-277, 2002.
- [31] E. Dulkeith, A.C. Morteani, T. Niedereichholz, T.A. Klar, J. Felderman, S.A. Levi, F.C.J.M. van Veggel, D.N. Reinhoudt, M. Moller, and D.I. Gittins, "Fluorescence Quenching of Dye Molecules near Gold Nanoparticles: Radiative and Nonradiative Effects," *Physical Review Letters*, **89**, (20), 203002-203005, 2002.
- [32] C. Fan, S. Wang, J.W. Hong, G.C. Bazan, K.W. Plaxco, and A.J. Heeger, "Beyond superquenching: Hyper-efficient energy transfer from conjugated polymers to gold nanoparticles," *Applied Physical Sciences*, **100**, (11), 6297-6301, 2003.
- [33] J. Gersten and A. Nitzan, "Spectroscopic properties of molecules interacting with small dielectric particles," *J. Chem. Phys.*, **75**, (3), 1139-1152, 1981.
- [34] A. Mooradian, "Photoluminescence of metals," *Physical Review Letters*, **22**, (5), 185-187, 1969.
- [35] G.P. Wiederrecht, "Near-field optical imaging of noble metal nanoparticles," *Euro. Phys. J.: Appl. Phys.*, **28**, (1), 3-18, 2004.
- [36] P. Apell and R. Monreal, "Photoluminescence of noble metals," *Physica Scripta*, **38**, (2), 174-179, 1988.
- [37] G.T. Boyd, Z.H. Yu, and Y.R. Shen, "Photoinduced luminescence from the noble metals and its enhancement on roughened surfaces," *Phys. Rev. B*, **33**, (12-15), 7923-7936, 1986.

- [38] A. Haes and R.P. Van Duyne, “A unified view of propagating and localized surface plasmon resonance biosensors,” *Analytical and Bioanalytical Chemistry*, **379**, (7-8), 920-930, 2004.